Journal of Visualized Experiments

Synthesis of Metal Nanoparticles Supported on Carbon Nanotube with Doped Co and N atoms and its Catalytic Applications in Hydrogen Production

--Manuscript Draft--

Article Type:	Methods Article - JoVE Produced Video
Manuscript Number:	JoVE62965R2
Full Title:	Synthesis of Metal Nanoparticles Supported on Carbon Nanotube with Doped Co and N atoms and its Catalytic Applications in Hydrogen Production
Corresponding Author:	Chi-Wing Tsang, Ph.D. Technological and Higher Education Institute of Hong Kong Hong Kong, N/A HONG KONG
Corresponding Author's Institution:	Technological and Higher Education Institute of Hong Kong
Corresponding Author E-Mail:	ctsang@vtc.edu.hk
Order of Authors:	Chi-Wing Tsang, Ph.D.
	Ka-Man Lee
	Pui-Ching Poon
	Yuanhao Wang
	Peter Shu-Wai Leung
	William Wai Yan Lam
	Weiqun Li
	Layla Mehdi
	Xiao-Ying Lu
	Eugene Yin Cheung Wong
	Yang Lu
Additional Information:	
Question	**Response**
Please specify the section of the submitted manuscript.	Chemistry
Please indicate whether this article will be Standard Access or Open Access.	Standard Access ($1400)
Please indicate the **city, state/province, and country** where this article will be **filmed**. Please do not use abbreviations.	Hong Kong
Please confirm that you have read and agree to the terms and conditions of the author license agreement that applies below:	I agree to the UK Author License Agreement (for UK authors only)
Please provide any comments to the journal here.	
Please confirm that you have read and agree to the terms and conditions of the video release that applies below:	I agree to the Video Release

TITLE:

Synthesis of Metal Nanoparticles Supported on Carbon Nanotube with Doped Co and N atoms and its Catalytic Applications in Hydrogen Production

AUTHORS AND AFFILIATIONS:

Pui-Ching Poon[1,#], Ka-Man Lee[1,#], Yuanhao Wang[2], William Wai Yan Lam[1], Peter Shu-Wai Leung[1], Xiao-Ying Lu[1], Weiqun Li[3], Layla B. Mehdi[3], Yang Lu[4], Chi-Wing Tsang[1,*], Eugene Yin Cheung Wong[2,*]

[1]Faculty of Science and Technology, Technological and Higher Education Institute of Hong Kong (THEi), Hong Kong 999077, China

[2]Department of Supply Chain and Information Management, The Hang Seng University of Hong Kong, Hong Kong 999077, Hong Kong 999077, China

[3]Department of Mechanical, Materials and Aerospace Engineering, University of Liverpool, Liverpool L69 3GQ, United Kingdom

[4]Laboratory of Building Environment and New Energy Resources, School of Civil Engineering, Faculty of Infrastructure Engineering, Dalian University of Technology, 116024, China

[#]These authors have contributed equally.

Email addresses of co-authors:

Pui-Ching Poon	(180054182@stu.thei.edu.hk)
Ka-Man Lee	(170637513@stu.thei.edu.hk)
Yuanhao Wang	(ywang@hsu.edu.hk)
Peter Shu-Wai Leung	(pswleung@thei.edu.hk)
William Wai Yan Lam	(williamlamwy@thei.edu.hk)
Xiao-Ying Lu	(xylu@thei.edu.hk)
Weiqun Li	(weiqunli@liverpool.ac.uk)
Layla B. Mehdi	(blmehdi@liverpool.ac.uk)
Yang Lu	(lvyang_dlut@163.com)
Chi-Wing Tsang	(ctsang@thei.edu.hk)
Eugene Yin Cheung Wong	(eugenewong@hsu.edu.hk)

[*]Corresponding authors:

Chi-Wing Tsang	(ctsang@thei.edu.hk)
Eugene Yin Cheung Wong	(eugenewong@hsu.edu.hk)

SUMMARY:

Here, we present a protocol to synthesize Co nanoparticles supported on carbon nanotubes with Co- and N- dopants for hydrogen productions.

ABSTRACT:

A method for facile synthesis of nanostructured catalysts supported on carbon nanotubes with atomically dispersed cobalt and nitrogen dopant is presented herein. The novel strategy is based

on a facile one-pot pyrolysis treatment of cobalt (II) acetylacetonate and nitrogen-rich organic precursors under Ar atmosphere at 800 °C, resulting in the formation of Co- and N- co-doped carbon nanotube with earthworm-like morphology. The obtained catalyst was found to have a high density of defect sites, as confirmed by Raman spectroscopy. Here, cobalt (II) nanoparticles were stabilized on the atomically dispersed cobalt- and nitrogen-doped carbon nanotubes. The catalyst was confirmed to be effective in the catalytic hydrolysis of ammonia borane, in which the turnover frequency was 5.87 mol $H_2 \cdot mol_{Co}^{-1} \cdot min^{-1,}$ and the specific hydrogen generation rate was determined to be 2447 mL $H_2 \cdot g_{Co}^{-1} \cdot min^{-1}$. A synergistic function between the Co nanoparticle and the doped carbon nanotubes was proposed for the first time in the catalytic hydrolysis of ammonia borane reaction under a mild condition. The resulting hydrogen production with its high energy density and minimal refueling time could be suitable for future development as energy sources for mobile and stationary applications such as road trucks and forklifts in transport and logistics.

INTRODUCTION:

Developing low-cost and highly efficient catalysts for renewable energy production remains one of the most critical and challenging problems to relieve the energy crisis. However, it is far from practical applications due to several concerns, such as large-scale production methods with reliable performance, high production cost, and long-standing stability to extend the service life of catalysts. Industry sectors, like transport and logistics, require energy production for vehicles and equipment with long operation hours, high powered energy supply, and minimal refueling time in achieving efficient operations[1–3]. Therefore, effective strategies have been extensively exploited to address the above technical challenges. For example, by regulating the electronic structure of the metal active sites and catalyst supports, designing the specific architecture of the metal nano-catalysts, fine-tuning metal compositions, functional group modification of anchored support, and varying the morphology to increase the number of intrinsic active sites. In the past few decades, nanoparticles (NPs) have dominated the fields of various heterogeneous catalysis, and the catalytic activities can be effectively tuned by varying the size of the NPs. Only until in recent years, highly dispersed single-atom catalysts (SACs) emerged to have excellent properties towards many catalysis reactions due to their unique electronic structure and coordination environment. Particularly, SACs have already demonstrated superior performances in energy conversion such as electrochemical reactions (HER, ORR, OER) and electrochemical energy systems (e.g., supercapacitors, rechargeable batteries)[4–6]. While both NPs and SACs have both advantages and limitations in catalytic applications, there do exist reactions that require both NPs and SACs in order to boost catalytic reactivity. For example, Ru NPs supported on Ni- and N-co-doped carbon nanotube superstructure could facilitate the high catalytic wet air oxidation of acetic acid[7]. This synergistic effect was also demonstrated by Pd_{1+NPs}/TiO_2 catalysts for highly selective ketone and aldehydes hydrogenation at room temperatures[8]. In order to accelerate the field of synergistic NPs and SACs catalysis and explore more on their catalytic applications, a facile way of catalyst synthesis is highly desirable, and the introduction of high loadings of the atomically dispersed active site remains a challenge due to the high tendency of the aggregation of SACs[9].

Several methods have been utilized to synthesize SACs for applications in the hydrogenation of nitroarenes[10], oxygen reduction reaction and hydrogen evolution reaction[11,12], lithium-oxygen batteries[13]. The most common strategy is the bottom-up approach, in which the metal precursors were absorbed, reduced, and immobilized on the defects of the corresponding support. Mononuclear metal complexes could also be first attached to the functional group of supports, followed by subsequent removal of the organic ligands, thus creating active metal sites for the catalytic process. Atomic layer deposition (ALD) is probably the most frequently used procedure for bottom-up fabrication by depositing a thin layer of film on the substrate with repeated exposure of reactants. Although the catalyst size could be precisely controlled and the reactivity could be greatly improved[14], the purity of the substrate was rather demanding, and the metal loading was relatively low, thus resulting in high production costs for practical applications. Various methods such as direct impregnation, co-precipitation, and deposition-precipitation, have been employed to immobilize metal nanoparticles onto the support surfaces, such as metal oxide and nitride, through surface charging effects. However, increasing metal loading usually leads to significant agglomeration and cluster formation of the metal atoms or nanoparticles. Therefore, usually, a very diluted metal solution is required, thus leading to low SACs loadings of the catalysts[15]. Amine ligands such as phenanthroline have been employed to undergo pyrolysis with metal precursors to prepare atomically dispersed metal catalysts with highly active Co-N_x active sites for the selective dehydrogenation of formic acid. However, the metal loading was relatively low (2–3 wt%) due to the limited number of available N atoms in the amine precursors[16].

In the past few decades, hydrogen has been regarded as a potential alternative to replace fossil fuels or hydrocarbons, such as coal, natural gas, and gasoline, due to the advantage of zero-emission of the former. Until now, about 94% of commercial hydrogen is still produced from the reforming process of fossil fuels, in which the process releases a great deal of greenhouse gas[17]. Therefore, hydrogen production from renewable resources such as water electrolysis is a way to solve the problem of depleted fossil resources and severe carbon emissions. However, the low hydrogen production efficiency has hindered their wider applications. Thus, to overcome this kinetic energy barrier for water-splitting, numerous efficient electrocatalysts have been discovered in the past decade[18]. Another issue is the storage problem due to the gaseous and explosive nature of hydrogen gas at ambient conditions. Physical storage methods such as compression will require the hydrogen to be compressed up to 700–800 bar, and cryogenic storage by liquefaction will require low temperature at -253 °C[19]. Although commercialized hydrogen fuel cell-powered vehicles have been successfully demonstrated, the storage problem is yet to be solved if the technology is to be used in wider applications, such as miniature devices and mini-fuel cells. Thus, storage methods of using chemical H materials have been one of the hot focuses in hydrogen energy research. Some examples of chemical H storage materials are ammonia borane (AB)[20], formic acid (FA)[21], ammonia gas[22], sodium alanate[23], and magnesium hydride[24]. Among these, AB has a low molecular weight (30.7 $g \cdot mol^{-1}$), high gravimetric and volumetric densities (196 $gH_2 \cdot kg^{-1}$ and 146 $gH_2 \cdot L^{-1}$, respectively). Besides, it is an air and moisture stable compound, non-toxic, and highly soluble in water. Metal nanoparticles on various supported materials have been widely used to release the three equivalents of hydrogen from AB, such as platinum- (Pt-), palladium- (Pd-), ruthenium- (Ru-), cobalt- (Co-), and nickel- (Ni-)

based catalysts. Co-based heterogeneous catalysts supported on carbon materials are especially attracting much attention due to their low cost, high abundance, and ease of recovery. Several synthetic strategies have been reported, such as the Co NPs supported on branched polyethylenimine-decorated graphene oxide[25]. The 3D structure with a large surface area ensures the stabilization of Co NPs maintaining at the 2–3 nm size range and prevented the aggregation of NPs. Another strategy is to use N-doped carbon materials to support Co NPs with small sizes. Using Co(salen)[26] and Co-MOF[27] (metal organic framework) as the precursors, Co NPs of 9.0 nm and 3.5 nm supported on N-doped porous carbon materials have been prepared respectively. The stability towards AB hydrolysis are high and the reactivity can maintain over 95% of the initial activity after 10 reaction runs. Recently, catalysts with hollow micro/nanostructures have been exploited for AB hydrolysis. These materials are conventionally prepared by hydrothermal methods and have been widely used for lithium-ion batteries, supercapacitors, chemical sensors, and heterogeneous catalysis research. Thus, the copper-cobalt synergy towards AB hydrolysis has been demonstrated by the hollow $CuMoO_4$-$CoMoO_4$[28], which gives a high TOF of 104.7 min^{-1}. Other highly structural-dependent examples include the core-shell CuO-NiO/Co_3O_4[29], the $Co_xCu_{1-x}Co_2O_4$@$Co_yCu_{1-y}Co_2O_4$ yolk-shell type[30], and the $Ni_{0.4}Cu_{0.6}Co_2O_4$ nanoarrays[31] were also found to be active towards AB hydrolysis. Another type of emerging materials known as heterostructured catalysts, such as MXenes and layered double hydroxides (LDHs), are increasingly being exploited for electrocatalytic and photocatalytic reaction[32–35]. These materials such as the NiFe-layered double hydroxide[36,37] and the CoB-N materials having N-doped carbon-cobalt boride heterointerfaces[38] are especially active for oxygen evolution and reduction reaction. In principle, they could be further exploited for hydrogen evolution reactions from hydrogen storage materials such as ammonia borane[39]. Maximizing the interaction between the catalysts and substrates is also another strategy for AB hydrolysis. Chiang et al. have utilized the surface oxide group of graphene oxide to form an initiated complex species with AB[40], thus $Ni_{0.8}Pt_{0.2}$/GO and rGO demonstrated excellent reactivity towards AB hydrolysis. The use of α-MoC as support for Co and Ni bimetallic catalysts assisted the activation of water molecules and achieved high TOF towards AB hydrolysis, which is four times higher than the commercial Pt/C catalyst[41].

Taking advantage of high N contents of the dicyandiamide and related C_3N_4 materials, a protocol for achieving a facile synthesis of cobalt NPs supported on highly dispersed Co- and N-doped carbon nanotubes is presented herein. The graduation *in-situ* formation of Co NPs from the formed atomically dispersed Co during the pyrolysis of C_3N_4 materials ensure that 1) Co NPs and Co dopants are highly dispersed; 2) Co NPs can be strongly anchored on the doped carbon supports and 3) Co NPs size can be carefully controlled by the temperature and time of the pyrolysis. The as-prepared Co/Co-N-CNT, as a result of the strongly anchored Co NPs and the ability of the Co dopants to lower the adsorption energy of water molecules, was found to have superior stability towards the hydrolysis of AB for hydrogen production. The details of the synthetic protocol of the catalysts and the measurement of the hydrogen production will be the focal point of this report.

PROTOCOL:

CAUTION: Readers are advised to carefully check the properties and toxicities of the chemicals described in this paper for the proper chemical handling from the relevant material safety data sheets (MSDS). Some of the chemicals used are detrimental to health, and special cares are to be taken. The impact of nanomaterials on human health is unknown and could pose safety and health risks. Inhalation and contact through the skin with these materials should be avoided. Safety precautions shall also be exercised, such as releasing the waste gas during the catalyst synthesis to the fume hood and catalyst performance evaluation with proper venting of the hydrogen gas. Personal protective equipment is advised to be worn at all times. Hydrogen is a potentially explosive gas with a very broad flammability range from 4%–74% in air. Care shall be taken to allow the hydrogen gas to vent properly to the atmosphere.

1. Synthesis of melem-C_3N_4 materials

1.1. Weigh out 280 g of dicyanamide (density = 1.4 $g \cdot cm^{-3}$) into an 800 mL beaker.

1.2. Place the beaker with the above solid into a muffle furnace and slowly raise the temperature from room temperature to 550 °C with a ramp of 5 $°C \cdot min^{-1}$.

1.3. Keep the temperature at 350 °C for 2 h, cool down the furnace by natural cooling.

1.4. Grind the obtained white solids into fine powder as the C_3N_4 materials in the melem form (DCD-350).

NOTE: The yield is 175 g.

2. Annealing the melem-C_3N_4 and $Co(acac)_2$ mixtures at different temperature

2.1. Mix 10.0 g of melem-C_3N_4 with 0.218 g of $Co(acac)_2$ [$Co(acac)_2$: melem-C_3N_4 = 1:200 (weight ratio)]. Grind and mix the two solids until the homogeneous color is observed.

2.2. Add 6 mL of citric acid solution (water: ethanol = 1:1, citric acid = 10 g·L-1) to the homogeneous mixture and further grind the materials.

2.3. Dry the materials in an oven at 60 °C for 6 h.

2.4. Place the materials into a square-shaped crucible and then into a tubular furnace.

2.5. Heat the materials at a heating rate of 2.6 $°C \cdot min^{-1}$ from room temperature to 800 °C and keep for 2 h under an Ar flow of 100 $mL \cdot min^{-1}$.

2.6. Slowly cool down the furnace by natural cooling.

2.7. Weight out the catalyst samples. Here, the yield was 0.65 g.

3. Measuring hydrogen release from ammonia borane hydrolysis

3.1. Set up the water-filled inverted cylinder system (**Supplementary Figure 1**).

3.2. Set up the 0.1 M H_2SO_4 washing solution.

3.3. Connect the Schlenk flask with the washing solution and the water-filled inverted cylinder.

3.4. Place 0.04 g of the catalyst into the Schlenk flask.

3.5. Prepare a solution of ammonia borane in water, with 0.04 g of ammonia borane in 0.948 mL of water (concentration = 0.04 $g \cdot mL^{-1}$).

3.6. Inject 1 mL of the NH_3BH_3 solution (40 $mg \cdot mL^{-1}$) to the reactor to initiate the hydrolysis reaction.

3.7. Monitor the drop in the water level as the reaction proceeds. Carefully record the production volume at designated times, e.g., each 5 s intervals.

3.8. Plot the graph of volume of H_2 production vs. time in minutes.

4. Kinetic studies

4.1. Determine the activation energy

4.1.1. Set the water bath temperature at 40 °C.

4.1.2. Place 0.04 g of the catalyst and 10 mL of water into the Schlenk flask and immerse into the water bath. Sonicate the solution at 40 kHz in an ultrasonic bath for 6 min.

4.1.3. Inject 1 mL of the NH_3BH_3 solution (40 $mg \cdot mL^{-1}$) to the reactor to initiate the hydrolysis reaction.

4.1.4. Record the time for completion of the hydrogen release.

4.1.5. Repeat steps 4.1.1–4.1.4 setting the water bath temperature at 35 °C.

4.1.6. Repeat the above experiment at 30 °C and 25 °C, respectively.

4.1.7. Plot the specific rate constant versus time on a graph using the following equation. A plot of ln k and 1/T should yield a straight line.

$$ln\ k_o = \frac{-E_a}{RT} + lnA$$

where k_o denotes the specific rate constant (mol $H_2 \cdot g_{Co}^{-1} \cdot min^{-1}$), R is the ideal gas constant (8.314 $kJ \cdot mol^{-1}$), T represents the reaction temperature (K), and A is the pre-exponential factor (mol H_2 $g_{Co}^{-1} \cdot min^{-1}$).

4.2. Determine the turnover frequency and specific hydrogen generation rate

4.2.1. Calculate the turnover frequency according to the following equation:

$$\mathrm{TOF} = \frac{n_{H_2}}{\Delta t \cdot n_M}$$

where n_{H2} is the moles of hydrogen produced, Δt is the time required for complete hydrogen release and n_M is the molar amount of metal in the catalyst.

4.2.2. Calculate the specific hydrogen generation rate according to the following equation[42,43]:

$$\mathrm{r}_B = \frac{\Delta V_{H_2}}{\Delta t \cdot \omega_M}$$

Where ΔV_{H2} is the volume of hydrogen produced, Δt is the time required for the initiating and stabilizing stages (e.g., the time where 70 mL of hydrogen generated for 40 mg ammonia borane, the time where 140 mL of hydrogen generated for 80 mg ammonia borane) and ω_M is the mass of metal in the catalyst.

4.3. Determine the relationship between [ammonia borane] and reaction rate

4.3.1. Set the water bath temperature at 40 °C.

4.3.2. Place 40 mg of the catalyst and 10 mL of water into the Schlenk flask and immerse into the water bath. Sonicate the solution at 40 kHz in an ultrasonic bath for 6 min.

4.3.3. Inject 1 mL of the NH_3BH_3 solution (40 $mg \cdot mL^{-1}$) to the reactor to initiate the hydrolysis reaction.

4.3.4. Record the time for completion of the hydrogen release.

4.3.5. Repeat step 4.3.3 injecting 2 mL of the NH_3BH_3 solution (i.e., 80 mg per 2 mL) to the reactor to initiate the hydrolysis reaction.

4.3.6. Repeat steps 4.3.1–4.3.4 with 0.5 mL and 0.25 mL of the NH_3BH_3 solution (40 mg/mL) respectively to record the time for completion of the hydrogen release.

4.3.7. Calculate the reaction rate according to the following equation[44]:

$$\text{reaction rate} = \frac{\Delta ml_{H_2}}{\Delta t}$$

where Δml_{H2} is the volume of hydrogen produced, Δt is the time required for 70 mL of hydrogen release.

4.3.8. Plot the ln rate vs. ln[ammonia borane] and determine the slope of the graph.

4.4. Determine the relationship between [catalysts] and production rate

4.4.1. Set the water bath temperature at 40 °C.

4.4.2. Place 40 mg of the catalyst and 10 mL of water into the Schlenk flask and immerse into the water bath. Sonicate the solution at 40 kHz in an ultrasonic bath for 6 min.

4.4.3. Inject 1 mL of the NH_3BH_3 solution (40 mg·mL^{-1}) to the reactor to initiate the hydrolysis reaction.

4.4.4. Record the time for completion of the hydrogen release.

4.4.5. Repeat steps 4.4.1–4.4.4 varying the amount of catalyst (20 mg, 40 mg, 60 mg, 80 mg) and inject 1 mL of the NH_3BH_3 solution (i.e., 40 mg·mL^{-1}) into the reactor to initiate the hydrolysis reaction.

4.4.6. Record the time for completion of the hydrogen release for using the above various catalyst amounts.

4.4.7. Calculate the reaction rate according to the following equation[44]:

$$\text{reaction rate} = \frac{\Delta ml_{H_2}}{\Delta t}$$

where Δml_{H2} is the volume of hydrogen produced, Δt is the time required for 70 mL of hydrogen release.

4.4.8. Plot the ln rate vs. ln[catalyst] and determine the slope of the graph.

5. Cycling performance test

5.1. Set the water bath temperature at 40 °C.

5.2. Place 0.04 g of the catalyst and 10 mL of water into the Schlenk flask and immerse into the water bath. Sonicate the solution at 40 kHz in an ultrasonic bath for 6 min.

5.3. Inject 1 mL of the NH_3BH_3 solution (40 $mg \cdot mL^{-1}$) to the reactor to initiate the hydrolysis reaction.

5.4. Record the time for completion of the hydrogen release.

5.5. Filter off the catalyst, washed with water (5 mL) three times, and then dry the catalyst in the oven (60 °C) for 3 h.

5.6. Place the catalyst in 10 mL of water and sonicate the solution at 40 kHz in an ultrasonic bath.

5.7. Repeat steps 5.1.3–5.1.5 for ten times.

5.8. Plot the hydrogen production volume vs. cycles.

6. Leaching experiment for metal NPs to obtain pure metal SAs CNT

6.1. Set the oil bath temperature at 80 °C.

6.2. Place 0.15 g of the catalyst and 50 mL of 0.5 M H_2SO_4 into the Schlenk flask and immerse into the oil bath.

6.3. Stir the reaction for 2 h.

6.4. Filter off the solid using a Buchner funnel and wash the solid with deionized water (3x in 10 mL each). Dilute the leachate further to 250 mL in a 250 mL volumetric flask.

6.5. Collect the metal nanoparticles-leached solids (which contain only Co-doped CNT) and dry at 60 °C in an oven.

7. Metal content determination using Inductively Coupled Plasma Optical Emission Spectroscopy (ICP-OES)

7.1. Determination of total cobalt metal content

7.1.1. Place approximately 0.02 g of as-prepared catalyst from section 2 into 50 mL of 2 M acid solution (HCl: HNO_3 = 3:1 mole ratio)[45,46] in a polytetrafluoroethylene-lined stainless-steel autoclave.

7.1.2. Place the polytetrafluoroethylene-lined container into the stainless steel bomb and secure the cap.

7.1.3. Place the bomb into an oven, set the temperature to 180 °C, and heat the bomb for 12 h.

7.1.4. Remove the bomb and empty the contents. Filter the solid and dilute the solute in a 250 mL volumetric flask with 200 mL of deionized water.

NOTE: The purpose of the dilution is to adjust the concentration of the ICP samples, which will fit into the metal standard concentration range, i.e., 0–40 ppm.

7.1.5. Run the ICP-OES test of the solution and calculate the total amount of Co in wt%.

7.2. Determination of the cobalt atoms content on the CNT

7.2.1. Place approximately 0.02 g of as-prepared catalyst from step 6.5 into 50 mL of 2 M acid solution (HCl: HNO_3 = 3:1 mole ratio)[45,46] in a polytetrafluoroethylene-lined stainless-steel autoclave.

7.2.2. Place the polytetrafluoroethylene-lined container into the stainless-steel bomb and secure the cap.

7.2.3. Place the bomb into an oven, set the temperature to 180 °C, and heat the bomb for 12 h.

7.2.4. Remove the bomb and empty the contents. Filter the solid and dilute the solute in a 250 mL volumetric flask with 200 mL of deionized water.

NOTE: The purpose of the dilution is to adjust the concentration of the ICP samples, which will fit into the metal standard concentration range, i.e., 0–40 ppm.

7.2.5. Run the ICP-OES test of the solution and calculate the amount of Co atom contents in wt%.

7.3. Determination of the cobalt nanoparticles (NPs) content

7.3.1. The difference between the metal content of 7.1.5 and 7.2.5 is the wt% of Co NPs.

REPRESENTATIVE RESULTS:

X-ray diffraction patterns (XRD) have been obtained to determine the crystallinity and size of the cobalt NPs. As shown in **Figure 1**, diffraction peaks corresponding to the (111), (200) and (220) planes (at 2θ of 44.2°, 51.5°, and 75.8° respectively) of the cubic phase of metallic cobalt were present in agreement with the JCPDS (Joint Committee for Powder Diffraction Standards) power diffraction file (card # 15-0806)[47]. The broad peak at 2θ of around 26° corresponding to the

graphitic carbon (N-CNTs) can be indexed to JCPDS card # 75-1621. The strong and sharp diffraction peaks indicate a well-defined crystalline structure.

[Place **Figure 1** here]

The structural defects and transformation can be illustrated in the Raman spectrum, as shown in **Figure 2**. The D band, which was attributed to the structural deformation of the sp^3-hybridized carbon vibrations, can be assigned to the peak at 1338 cm^{-1}. The G band, which was due to the E_{2g} scattering vibrational mode of first-ordered scattering in a hexagonal lattice by the sp^2-hybridized carbon domain, can be assigned to the peak at 1585 cm^{-1}. The ratio of I_D/I_G was determined to be 1.13, indicating that there was a high degree of defect density in the sample. The defects could be caused by the anchored Co and N dopants in the carbon structure of the as-prepared catalyst[48,49]. In addition, there were three peaks detected at 475.4 cm^{-1}, 519.3 cm^{-1}, and 674.0 cm^{-1} which can be assigned to the cobalt nitride phase[50]. This indicated that partial nitridation of the Co NPs occurred during the NH_3(g) formation from g-C_3N_4 decomposition at around 700 °C[49]. There was no observable change in the appearance of the spectrum after the AB hydrolysis reaction, suggesting the high stability of the as-prepared catalyst.

[Place **Figure 2** here]

As shown in **Figure 3A**, the orbital peaks of the XPS survey spectrum signified the presence of N, C, and Co elements. The high-resolution electron spectroscopy for chemical analysis (ESCA) of each element further indicates the chemical states of the elements. Three characteristics peaks, namely, the metallic Co, Co-N, and Co^{2+}, are shown by the spatial resolution of the Co $2p_{3/2}$ XPS profile as in **Figure 3B**. The peaks corresponding to metallic Co, Co^{2+} (probably due to partial surface oxidation of the Co nanoparticles) and Co-N_X were located at 778.2 eV, 779.8 eV, and 781.1 eV, respectively, while the Co $2p_{1/2}$ XPS indicated the presence of Co^{2+} located at 795.8 eV. The deconvolution of the N1s high-resolution profile in **Figure 3C** showed that four peaks centered at 397.8 eV, 398.9 eV, 400.6 eV, and 402.9 eV were corresponding to C-N-C, Co-N, C-N-H, and graphitic N, respectively. The relatively stronger peak at 397.8 eV could be attributed to the presence of the strong interaction of metallic cobalt with nitrogen atoms[49,51], which could be either cobalt nanoparticles or/and cobalt dopants. As shown in **Figure 3D**, the ESCA spectrum of C1s can be resolved into three main peaks, indicating the different hybridization of carbon atoms during the formation of the carbon nanotube structures. The peaks centered at around 285 eV, 286 eV, and 290 eV could be attributed to C-C sp^3, C-C $sp^{2,}$ and C=N, respectively.

[Place **Figure 3A–D** here]

The specific surface area and pore size distribution of the Co/Co-N-CNT support were measured from a nitrogen adsorption-desorption isotherm at liquid nitrogen temperature (77 K). As shown in **Figure 4A**, the adsorption-desorption isotherm demonstrated a clear hysteresis look of type IV according to IUPAC nomenclature, with a specific surface area S_{BET} of 42.02 $m^2 \cdot g^{-1}$. The total pore volume of the pores less than 391.6 nm diameter at P/P_o is 0.25 $cm^3 \cdot g^{-1}$. The average pore size

distribution was determined to be 3.6 nm on the basis of the Barrett-Joyner-Halenda (BJH) methods, as shown in **Figure 4B**.

[Place **Figure 4A–B** here]

The structural and compositional characterization results of the Co/Co-N-CNT sample annealed at 800 °C were given in **Figure 5**. Here, the length of the convoluted carbon nanofiber was up to 5 μm and the tubular nanostructures could be clearly observed in **Figures 5A–B** and **Figure 6**. The Co nanoparticle, resulting from the catalyzing growth of the nanofiber[52,53], was located at the tip of the N-doped nanofiber. This could be clearly seen from HRTEM (JEM-2100Plus, JEOL) images in **Figures 5A–B** and the EDS mapping was also shown in **Figure 5C**. Such Co nanoparticle was wrapped by a few layers of graphitic carbon, as shown in **Figure 5D** and **Figure 5F**. The d-spacing of the graphitic carbon interlayer was around 3.46 Å, which was assigned to the (002) lattice plane of graphitic carbon. The crystalline structure of the Co nanoparticle was characterized by selected area electron diffraction (SAED) pattern from the $[11\bar{2}]$ zone axis, as revealed in **Figure 5E**. The lattice planes of (111), $(2\bar{2}0)$ and $(3\bar{1}1)$ of the crystalline Co were indexed accordingly. The main body of the carbon nanofiber is endowed with graphitic carbon layers of different orientations, as shown in **Figures 5G** and **Figure 5I**. The diffraction rings in **Figure 5H** confirmed the typical planes {002}, {101} and {110} of the graphitic carbon. Image obtained with scanning electron microscopy is shown in **Figure 6.**

[Place **Figure 5A–I** and **Figure 6** here]

The total metal content determined by ICP-OES was found to be 25.1 wt%, with 9.7 wt% of Co NPs and 15.4 wt% of Co dopants on the CNT, as shown in **Table 1**. The presence of Co NPs was probably due to the high loading of metal precursor $Co(acac)_2$ used in the synthesis.

[Place **Table 1** here]

The catalytic performance of the catalyst towards the hydrolysis of AB was given in **Figure 7**. The catalyst first underwent an activation process, probably due to the gradual formation of the HO-Co-N_2 active phase from Co SAs[54]. Finally, when the activation process was stabilized, the reaction finished in 3.8 min to release 2.94 equivalents of hydrogen, close to the theoretical value (3.0 equivalents of hydrogen). The turnover frequency (TOF) was determined to be 5.87 mol $H_2 \cdot mol_{Co}^{-1} \cdot min^{-1}$, and the specific hydrogen generation rate was determined to be 2447 mL $H_2 \cdot g_{Co}^{-1} \cdot min^{-1}$.

To understand the rate law of the reaction, the correlation of the rate and the amount of catalyst and ammonia borane was estimated, respectively. As shown in **Figure 8**, the ln rate Vs. ln [AB] and ln [catalyst] were plotted, respectively. The rate showed a slight dependence on ammonia borane, and the reaction order of the catalyst was about 0.4, which was quite different from most other reported rate law in the hydrolysis of ammonia borane but is similar to the one reported on the AB hydrolysis by CoP nanoparticles, reported as 0.6 due to the longer induction time of AB on the catalyst[55]. The rate law is thus determined to be rate = $k[catalyst]^{1.3}[AB]^{0.4}$. The activation energy (E_a) was determined to be 42.8 $kJ \cdot mol^{-1}$, as shown in **Figure 9**.

To verify the high stability of the as-prepared catalyst, cycling performance was also tested for 15 cycles. Ammonia borane was continuously added to the catalyst solution, and it was found that until the 10th time of AB addition, there was no obvious decline in the catalytic performance, as shown in **Figure 10A–C**, confirming that the synthesis strategy used in this study could achieve strong anchorage of nanoparticles on the CNT support. The NPs enclosed by the graphitic carbon of CNT could effectively prevent metal NPs agglomeration. Finally, the formation of the HO-Co-N_2 complex species[54] on the CNT at optimal pH effectively lowered the adsorption energy of water molecules onto the CNT for a hydrolysis reaction. During the recycling, as more ammonia borane was added, the reaction media reached an optimal pH in which all of the Co dopants were activated. This was demonstrated by the gradual increase in the specific hydrogen generation rate from 2447 ml $H_2 \cdot g\ Co^{-1}\ min^{-1}$ to over 3500 ml $H_2 \cdot g_{Co}^{-1} \cdot min^{-1}$ at the 7th catalytic reaction. The XRD results showed that (**Supplementary Figure 2**) the state of Co nanoparticles remains unchanged after the recycles. The detailed mechanism will be discussed in the following section.

[Place **Figure 7–Figure 10** here]

FIGURE AND TABLE LEGENDS:

Figure 1: XRD pattern of 0.5 wt% Co/CoN$_x$-CNT support. The black square symbol represents the crystal plane of Co.

Figure 2: Raman spectrum of 0.5 wt% Co/CoN$_x$-CNT support. ID/IG represents the ratio of the height of the peaks of D band and G band, respectively.

Figure 3: Typical XPS spectra of 0.5 wt% Co/CoN$_x$-CNT support. (**A**) XPS survey, (**B**) Co2p, (**C**) N1s and (**D**) C1s.

Figure 4: Adsorption-desorption isotherm and size distribution. (**A**) Adsorption-desorption isotherm of 0.5 wt% Co/CoNx-CNT materials. (**B**) Size distribution of 0.5 wt% Co/Co SACs-N-CNT determined from Barrett-Joyner-Halenda (BJH) method.

Figure 5: Transmission Emission Microscopy. (**A**, **B**) HRTEM images and (**C**) EDS mapping of the Co/Co-N-CNT. (**D**) HRTEM image and (**E**) SAED pattern of the Co nanoparticle at the tip of the CNT. (**F**) HRTEM image of the graphitized carbon layers wrapping the Co nanoparticle. (**G**) HRTEM image, (**H**) SAED pattern, and (**I**) HRTEM image of the CNT. The dashed orange and yellow squares indicate the location of (**F**) in (**D**) and (**I**) in (**G**), respectively.

Figure 6: Scanning Electron Microscopy. FE-SEM images of 0.5 wt% Co/CoNx-CNT support.

Figure 7: The catalytic performance of 0.5 wt% Co/Co SACs during AB hydrolysis. (**A**) Before and after activation, (**B**) TOF ratio at these two conditions.

Figure 8: Kinetics studies. (**A**) Plots of the time of dehydrogenation of AB at various AB concentrations. (**B**) Plot of the rate of H_2 generation at various concentrations of AB in natural

logarithmic scale. (**C**) Plots of the time of dehydrogenation of AB at various amounts of catalysts. (**D**) Plot of the rate of H_2 generation at various concentrations of catalyst in natural logarithmic scale.

Figure 9: Kinetics studies. (**A**) Plots of the time of dehydrogenation of AB at various temperatures; (**B**) Arrhenius plots derived from the obtained kinetic data.

Figure 10: Cyclic performance studies. (**A**) Recycling of 0.5 wt% Co/Co SACs catalyst (40 mg) in water (10 mL), with the addition of AB (1.30 mmol) to the system at 313 K in each cycle. (**B**) TOF ratio at each recycle. (**C**) Specific generation rate.

Figure 11: Proposed mechanism for the initiation step of ammonia borane hydrolysis by Co/Co-N-CNT catalyst. It was proposed that water molecules were first adsorbed on the activated Co single atoms, followed by interacting with the activated B-H bonds of the ammonia borane molecules.

Table 1: The total metal content determined by ICP-OES.

Supplementary Figure 1: Setup for the measurement of the volume of hydrogen release from the hydrolysis of ammonia borane. The measurement was recorded after the ammonia borane solution was fully injected into the reaction flask. Sulfuric acid was used to wash any residual ammonia gas which may be produced during the hydrolysis reaction. The volume displaced was recorded on a 10 s interval as the water level dropped inside the inverted cylinder.

Supplementary Figure 2: XRD pattern of 0.5 wt% Co/CoN_x-CNT support after 15 recycles. The state of Co nanoparticles remains unchanged.

DISCUSSION:

The pyrolysis method has become one of the powerful strategies in the synthesis of one-dimensional nanomaterial on various heteroatom-doped solid supports with controlled sizes of NPs. For example, the nanospace-confined pyrolysis strategy was reported by Guo et al.[56]. Briefly, the pre-treated MWCNTs, cobalt, and phosphorus precursors were pyrolysis at 800 °C under N_2 atmosphere, and the CoP NPs supported on N-CNT can be obtained. The presence of the micro-pores can act as the pathway for Co and P precursors to permeate during the pyrolysis and coordinate with the C and N atoms around the pores. This strategy could effectively control the size of NPs and inhibit their aggregation. Controlled growth of NPs could also be prepared by the transformation of SAs through slow aggregation. Previously, Ni-SA-N-CNT was also prepared by one-pot pyrolysis method with Ni precursor and dicyandiamide[52]. Ni SAs loading up to 20.3% was obtained at 800 °C under Ar, and it was found that at 900 °C small amount of Ni NPs started to form. In contrast, for Co SAs synthesis, it was found that as early as 700 °C, Co NPs were already observed, and it was found that pyrolysis at 800 °C for 2 h, 9.7 wt% of Co NPs were formed with about 15.4 wt% of Co SAs remaining. In addition, Co nanoparticle was uniformly wrapped by a few layers of graphitic carbon, as shown in **Figure 5D** and **Figure 5F**. The few layers of graphitic carbon, which was considered a protective coating for nanoparticles, could effectively inhibit the

608 further growth of the NPs and prevent further agglomeration after the ammonia borane
609 hydrolysis reactions.
610
611 Given the fact that High-angle annular dark-field (HAADF) imaging may not always be available
612 to detect the atomic dopants, a combined technique of XRD and ICP-OES will be useful for
613 preliminary screening of the presence of atomic dopants in the catalyst samples. The NPs were
614 usually well-observed as strong and sharp peaks, while SAs were generally shown as broad and
615 weak peaks in the XRD spectrum; therefore, closely monitoring the XRD spectrum ensures the
616 formation of the Co NPs. In addition, since NPs could be easily leached out by reacting with dilute
617 acid solution[16], as shown in section 6 of the protocol, the amount of the respective NPs and SAs
618 could be estimated unequivocally. This protocol ensures the catalysts have the Co dopant
619 components before sending them to HAADF for imaging.
620
621 Different from the reported "one-pot" pyrolysis method to prepare SAs CNT, DCD-350 was first
622 prepared by decomposition of the dicyandiamide in a muffle furnace at 350 °C to prepare the
623 melem-C_3N_4 materials (*m*-C_3N_4). The reason was due to the formation of a large amount of gas
624 and solid materials during the decomposition of dicyandiamide, presumably NH_3(g) and
625 ammonium salts. Therefore, the one-pot was slightly modified to a two-step procedure to avoid
626 too many solids being deposited in the tubular furnace at elevated temperatures, which may
627 cause blocking of the gas outlet of the furnace.
628
629 The formation mechanism of the earthworm-shaped CNT was believed to undergo a Co metal-
630 catalyzed reaction with the further decomposition of the *m*-C_3N_4. After the *m*-C_3N_4 and Co
631 precursor was completely mixed, at 650 °C, the *m*-C_3N_4 slowly transformed to the *g*-C_3N_4 form.
632 At 700 °C, Co SAs within the *g*-C_3N_4 molecules began to be thermally activated and became more
633 mobile. The thermal movement of Co SAs then creates internal stresses, which curl up the layered
634 Co-*g*-C_3N_4 layers to create a seamless graphitic cylindrical network, exhibited as an earthworm-
635 shaped CNT, as shown in the FE-SEM images in **Figure 6**. Increasing the nominal ratio of Co
636 precursor to DCD-350 from 1:200 to 1:33.3 greatly impacts the final morphology of the CNT
637 catalysts. It is believed that during the nitridation treatment of Co-SA/C-CNT, more defect density
638 can be created caused by the anchored implementation of Co SAs and N dopants in the carbon
639 structure[49]. Since Co precursor to DCD-350 of 1:200 could lead to more NH_3 generation during
640 pyrolysis; as a result, the D band and G band observed in **Figure 2** was greater than 1 while for
641 the ratio of 1:33.3, the ratio of D: G dropped below 1. This could explain the defect of the
642 nanotube was due to nitridation. In addition, the presence of the Co nitride peaks indicated the
643 presence of partial nitrification of the Co NPs; however, no such peaks were observed for the
644 catalyst with the ratio of 1:33.3. Therefore, the ratio of Co precursor to *m*-C_3N_4 can be used to
645 control defect density, while the Raman spectrum can be used to monitor this.
646
647 The synergy of NPs and SAs on catalyst support was very specific to reaction types, and therefore
648 understanding the AB hydrolysis mechanism can provide insight into effective catalyst design and
649 explore more useful applications for NPs-SAs catalysts. Several AB hydrolysis mechanisms were
650 proposed by different research groups. Fu et al. proposed the formation of an intermediate
651 $BH_3OH^-NH_4^+$ on the surface of the Ni_2P catalysts and followed by the subsequent attack of H_2O to

produce hydrogen molecules[57]. Xu et al. reported that the AB molecule interacts with the metal NPs surface to form an activated complex, and this should be the rate-determining step (RDS)[58]. The ammonia borane molecule on the surface of the metal NPs was first attacked by an H_2O molecule, followed by the concerted dissociation of the B-N bond. Hydrogen was then released with the concomitant production of borate ion on the metal NPs surface (-$B(OH)H_2^*$, -$B(OH)_2H^*$and -$B(OH)_3^*$). Jagirdar et al. reported the formation of a transient M-H bond after the attack of H_2O on the boron atom of AB, followed by the reaction of another H_2O molecule on the M-H bond to release hydrogen molecule[59]. Using D_2O as the solvent to study the kinetic isotope effect, Fu et al. confirmed that half of the released hydrogen came from H_2O, and half of the hydrogen comes from AB[55]. Chen et al. first proposed the S_N2 mechanism, where H_2O and AB are first adsorbed on the catalyst surface of $NiCo_2P_2$. Under the attack of OH^* molecule on the B atom to produce a series of intermediates such as $B(OH)H_3^*$, $B(OH)_2H_2^*$and $B(OH)_3H^*$ (i.e., OH^* + $BH_3NH_3^* \rightarrow B(OH)_3H^* + NH_3^*$). The $B(OH)_3H^*$ species then dissociate to release H^*, and $B(OH)H_2^*$ recombine with NH_3^* to form the $NH_3B(OH)H_2^*$, and the process is repeated until all three equivalent of hydrogen were released. Although the mechanism by different catalysts may slightly differ, the involvement of H_2O molecules was critical to the rate of the hydrolysis reactions. It is proposed that as the hydrolysis of AB proceeds, the reaction media become slightly alkaline, which facilitated the formation of the HO^*-Co-N_2 species by the oxidative addition of H_2O molecules, as shown in **Figure 11**. This species could lower the adsorption energy of H_2O molecules. At the same time, the abundant Co-N_x active site could donate electrons to the Co NPs, making them more active to activate AB through oxidative addition[60,61]. The H atom from both the AB and H_2O could then undergo reductive elimination to release H_2. Future work will be conducted to modulate the alkalinity of the reaction media to optimize the AB and H_2O adsorption kinetics for achieving better catalytic performance.

[Place **Figure 11** here]

In summary, a type of heterogeneous catalyst composed of both Co NPs and Co SAs supported on earthworm-like CNT nanostructure was demonstrated with a facile synthesis strategy. It has been found to successfully prepare the nano-catalyst with an abundant amount of both NPs and SAs and high defect density. Above all, the as-prepared nano-catalyst exhibited excellent activity and stability towards the hydrolysis reaction of ammonia borane for hydrogen gas production, demonstrating the successful catalyst design through combined functions by both NPs and SAs. The demonstrated high stability could facilitate hydrogen production with more reliable performance for the high-powered and stable requirement of industrial applications, such as cargo transportation through truck and forklift in the transport and logistics sector.

ACKNOWLEDGMENTS:

This work was fully funded by Hong Kong University Grants Committee - Institutional Development Scheme (IDS) Collaborative Research Grant, grant number UGC/IDS(C)14/B(E)01/19, the Faculty Development Scheme (FDS), grant number UGC/FDS25/E08/20 and partially funded by the Institutional Development Scheme (IDS), grant number UGC/IDS(R)11/20.

DISCLOSURES:

We have nothing to disclose.

REFERENCES:

1. Di Ilio, G., Di Giorgio, P., Tribioli, L., Bella, G., Jannelli, E. Preliminary design of a fuel cell/battery hybrid powertrain for a heavy-duty yard truck for port logistics. *Energy Conversion and Management.* **243** (2021).
2. Imdahl, C. et al. Potentials of hydrogen technologies for sustainable factory systems. *28th CIRP Conference on Life Cycle Engineering*. 583–588 (2021).
3. Keller, A. V., Karpukhin, K. E., Kolbasov, A. F., Kozlov, V. N. Analysis of hydrogen use as an energy carrier in transport. *IOP Conference Series: Materials Science and Engineering.* **1159**, 012087 (2021).
4. Sun, B. -W., Li, H. -J., Yu, H. -Y., Qian, D. -J., Chen, M. In situ synthesis of polymetallic Co-doped *g*-C_3N_4 photocatalyst with increased defect sites and superior charge carrier properties. *Carbon.* **117**, 1–11 (2017).
5. Zhang, Y. et al. Biomass chitosan derived cobalt/nitrogen-doped carbon nanotubes for the electrocatalytic oxygen reduction reaction. *Journal of Materials Chemistry A.* **6** (14), 5740–5745 (2018).
6. Sun, J. -F. et al. Isolated single atoms anchored on N-doped carbon materials as a highly efficient catalyst for electrochemical and organic reactions. *ACS Sustainable Chemistry & Engineering.* **8** (39), 14630–14656 (2020).
7. Jin, C. et al. Single-atom nickel confined nanotube superstructure as support for catalytic wet air oxidation of acetic acid. *Communications Chemistry.* **2** (1) (2019).
8. Kuai, L. et al. Titania supported synergistic palladium single atoms and nanoparticles for room temperature ketone and aldehydes hydrogenation. *Nature Communication.* **11** (1), 48 (2020).
9. Yang, X. -F. et al. Single-atom catalysts: A new frontier in heterogeneous catalysis. *Accounts of Chemical Research.* **46** (8), 1740–1748 (2013).
10. Sun, X. et al. Single cobalt sites in mesoporous N-doped carbon matrix for selective catalytic hydrogenation of nitroarenes. *Journal of Catalysis.* **357**, 20–28 (2018).
11. Sun, T. et al. Single-atomic cobalt sites embedded in hierarchically ordered porous nitrogen-doped carbon as a superior bifunctional electrocatalyst. *Proceedings of the National Academy of Sciences of the United States of America.* **115** (50), 12692-12697 (2018).
12. Wan, G. et al. Engineering single-atom cobalt catalysts toward improved electrocatalysis. *Small.* **14** (15), e1704319 (2018).
13. Wang, P. et al. Atomically dispersed cobalt catalyst anchored on nitrogen-doped carbon nanosheets for lithium-oxygen batteries. *Nature Communication.* **11** (1), 1576 (2020).
14. Yan, H. et al. Bottom-up precise synthesis of stable platinum dimers on graphene. *Nature Communication.* **8** (1), 1070 (2017).
15. Qiao, B. et al. Single-atom catalysis of CO oxidation using Pt_1/FeOx. *Nature Chemistry.* **3** (8), 634–641 (2011).
16. Tang, C. et al. A stable nanocobalt catalyst with highly dispersed CoN_x active sites for the selective dehydrogenation of formic acid. *Angewandte Chemie International Edition English.* **56** (52), 16616–16620 (2017).

17. Gnanapragasam, N. V., Rosen, M. A. A review of hydrogen production using coal, biomass and other solid fuels. *Biofuels.* **8** (6), 725–745 (2017).
18. Wang, S., Lu, A., Zhong, C. J. Hydrogen production from water electrolysis: role of catalysts. *Nano Converg.* **8** (1), 4 (2021).
19. Demirci, U. B. About the technological readiness of the H_2 generation by hydrolysis of B(−N)−H compounds. *Energy Technology.* **6** (3), 470–486 (2018).
20. Wu, H. et al. Metal-catalyzed hydrolysis of ammonia borane: Mechanism, catalysts, and challenges. *International Journal of Hydrogen Energy.* **45** (55), 30325–30340 (2020).
21. Singh, A. K., Singh, S., Kumar, A. Hydrogen energy future with formic acid: a renewable chemical hydrogen storage system. *Catalysis Science & Technology.* **6** (1), 12–40 (2016).
22. Grinberg Dana, A., Shter, G. E., Grader, G. S. Nitrogen-based alternative fuels: Progress and future prospects. *Energy Technology.* **4** (1), 7–18 (2016).
23. Ley, M. B., Meggouh, M., Moury, R., Peinecke, K., Felderhoff, M. Development of hydrogen storage tank systems based on complex metal hydrides. *Materials (Basel).* **8** (9), 5891–5921 (2015).
24. Wang, H., Lin, H. J., Cai, W. T., Ouyang, L. Z., Zhu, M. Tuning kinetics and thermodynamics of hydrogen storage in light metal element based systems – A review of recent progress. *Journal of Alloys and Compounds.* **658**, 280–300 (2016).
25. Li, M., Hu, J., Lu, H. A stable and efficient 3D cobalt-graphene composite catalyst for the hydrolysis of ammonia borane. *Catalysis Science & Technology.* **6** (19), 7186–7192 (2016).
26. Wang, H., Zhao, Y., Cheng, F., Tao, Z., Chen, J. Cobalt nanoparticles embedded in porous N-doped carbon as long-life catalysts for hydrolysis of ammonia borane. *Catalysis Science & Technology.* **6** (10), 3443–3448 (2016).
27. Zhou, L. et al. Ultrasmall cobalt nanoparticles supported on nitrogen-doped porous carbon nanowires for hydrogen evolution from ammonia borane. *Materials Horizons.* **4** (2), 268–273 (2017).
28. Feng, Y. et al. Sea-urchin-like hollow CuMoO4–CoMoO4 hybrid microspheres, a noble-metal-like robust catalyst for the fast hydrogen production from ammonia borane. *ACS Applied Energy Materials.* **4** (1), 633–642 (2021).
29. Liao, J. et al. CuO–NiO/Co3O4 hybrid nanoplates as highly active catalyst for ammonia borane hydrolysis. *International Journal of Hydrogen Energy.* **45** (15), 8168–8176 (2020).
30. Lu, D. et al. A simple and scalable route to synthesize Cox Cu1- x Co2 O4 @Coy Cu1- y Co2 O4 yolk-shell microspheres, a high-performance catalyst to hydrolyze ammonia borane for hydrogen production. Small. 15 (10), e1805460 (2019).
31. Feng, Y. et al. Durable and high performing Ti supported Ni0.4Cu0.6Co2O4 nanoleaf-like array catalysts for hydrogen production. *Renewable Energy.* **169**, 660–669 (2021).
32. Prabhu, P., Jose, V., Lee, J. M. Heterostructured catalysts for electrocatalytic and photocatalytic carbon dioxide reduction. *Advanced Functional Materials.* **30** (24) (2020).
33. Wang, H. et al. Electronic modulation of non-van der Waals 2D electrocatalysts for efficient energy conversion. *Advanced Materials.* **33** (26), e2008422 (2021).
34. Wang, H., Lee, J. -M. Recent advances in structural engineering of MXene electrocatalysts. *Journal of Materials Chemistry A.* **8** (21), 10604–10624 (2020).
35. Prabhu, P., Lee, J. M. Metallenes as functional materials in electrocatalysis. *Chemical Society Reviews.* **50** (12), 6700–6719 (2021).

784 36. Lin, Y. et al. Co-induced electronic optimization of hierarchical NiFe LDH for oxygen
785 evolution. *Small.* **16** (38), e2002426 (2020).
786 37. Li, M. et al. Gd-induced electronic structure engineering of a NiFe-layered double
787 hydroxide for efficient oxygen evolution. *Journal of Materials Chemistry A.* **9** (5), 2999–3006
788 (2021).
789 38. Jose, V. et al. Highly efficient oxygen reduction reaction activity of N-doped carbon–cobalt
790 boride heterointerfaces. *Advanced Energy Materials.* **11** (17) (2021).
791 39. Qiu, X. et al. Hydrogen generation from ammonia borane hydrolysis catalyzed by
792 ruthenium nanoparticles supported on Co–Ni layered double oxides. *Sustainable Energy & Fuels.*
793 **5** (8), 2301–2312 (2021).
794 40. Prabu, S., Chiang, K.-Y. Improved catalytic effect and metal nanoparticle stability using
795 graphene oxide surface coating and reduced graphene oxide for hydrogen generation from
796 ammonia–borane dehydrogenation. *Materials Advances.* **1** (6), 1952–1962 (2020).
797 41. Ge, Y. et al. Maximizing the synergistic effect of CoNi catalyst on a-MoC for robust
798 hydrogen production. *Journal of the American Chemical Society.* **143** (2), 628–633 (2020).
799 42. Duan, S. et al. Magnetic Co@g-C_3N_4 core-shells on rGO sheets for momentum transfer
800 with catalytic activity toward continuous-flow hydrogen generation. *Langmuir.* **32** (25), 6272–
801 6281 (2016).
802 43. Zhang, H. et al. Birdcage-type CoO_x-carbon catalyst derived from metal–organic
803 frameworks for enhanced hydrogen generation. *ACS Sustainable Chemistry & Engineering.* **7** (11),
804 9782–9792 (2019).
805 44. Semiz, L. Dehydrogenation of ammonia borane by dealloyed ruthenium catalysts.
806 *Inorganic and Nano-Metal Chemistry.* **51** (1), 20–26 (2020).
807 45. Bulut, A. et al. Carbon dispersed copper-cobalt alloy nanoparticles: A cost-effective
808 heterogeneous catalyst with exceptional performance in the hydrolytic dehydrogenation of
809 ammonia-borane. *Applied Catalysis B: Environmental.* **180**, 121–129 (2016).
810 46. Akbayrak, S., Tonbul, Y., Özkar, S. Ceria supported rhodium nanoparticles: Superb catalytic
811 activity in hydrogen generation from the hydrolysis of ammonia borane. *Applied Catalysis B:*
812 *Environmental.* **198**, 162–170 (2016).
813 47. Powder diffraction file PDF-2 data base international center for diffraction data JCPDS-
814 ICDD 1999 in JCPDS database. *International Centre for Diffraction Data* at <icdd.com> (2021)
815 48. Zhang, J., Zhao, Z., Xia, Z., Dai, L. A metal-free bifunctional electrocatalyst for oxygen
816 reduction and oxygen evolution reactions. *Nature Nanotechnology.* **10** (5), 444–452 (2015).
817 49. Cao, B. et al. Tailoring the *d*-band center of N-doped carbon nanotube arrays with Co_4N
818 nanoparticles and single-atom Co for a superior hydrogen evolution reaction. *NPG Asia Materials.*
819 **13** (1) (2021).
820 50. Varga, T. et al. Co_4N/nitrogen-doped graphene: A non-noble metal oxygen reduction
821 electrocatalyst for alkaline fuel cells. *Applied Catalysis B: Environmental.* **237**, 826–834 (2018).
822 51. Li, H., Gan, S., Wang, H., Han, D., Niu, L. Intercorrelated superhybrid of AgBr supported on
823 graphitic-C_3N_4-decorated nitrogen-doped graphene: High engineering photocatalytic activities for
824 water purification and CO_2 reduction. *Advanced Materials.* **27** (43), 6906–6913 (2015).
825 52. Zhao, S. et al. One-pot pyrolysis method to fabricate carbon nanotube supported Ni single-
826 atom catalysts with ultrahigh loading. *ACS Applied Energy Materials.* **1** (10), 5286–5297 (2018).
827 53. Dilpazir, S. et al. Cobalt single atoms immobilized N-doped carbon nanotubes for

enhanced bifunctional catalysis toward oxygen reduction and oxygen evolution reactions. *ACS Applied Energy Materials.* **1** (7), 3283–3291 (2018).

54. Cao, L. et al. Identification of single-atom active sites in carbon-based cobalt catalysts during electrocatalytic hydrogen evolution. *Nature Catalysis.* **2** (2), 134–141 (2018).

55. Fu, Z. C. et al. Highly efficient hydrolysis of ammonia borane by anion ($^{-}$OH, F^{-}, Cl^{-})-tuned interactions between reactant molecules and CoP nanoparticles. *Chemical Communications*. **53** (4), 705–708 (2017).

56. Hou, C. -C. et al. Tailoring three-dimensional porous cobalt phosphides templated from bimetallic metal–organic frameworks as precious metal-free catalysts towards the dehydrogenation of ammonia-borane. *Journal of Materials Chemistry A.* **7** (14), 8277–8283 (2019).

57. Peng, C. Y. et al. Nanostructured Ni_2P as a robust catalyst for the hydrolytic dehydrogenation of ammonia-borane. *Angewandte Chemie International Edition English.* **54** (52), 15725–15729 (2015).

58. Xu, Q., Chandra, M. Catalytic activities of non-noble metals for hydrogen generation from aqueous ammonia–borane at room temperature. *Journal of Power Sources.* **163** (1), 364–370 (2006).

59. Kalidindi, S. B., Sanyal, U., Jagirdar, B. R. Nanostructured Cu and Cu@Cu_2O core shell catalysts for hydrogen generation from ammonia–borane. *Physical Chemistry - Chemical Physics.* **10**, 5870–5874 (2008).

60. Ning, X., Yu, H., Peng, F., Wang, H. Pt nanoparticles interacting with graphitic nitrogen of N-doped carbon nanotubes: Effect of electronic properties on activity for aerobic oxidation of glycerol and electro-oxidation of CO. *Journal of Catalysis.* **325**, 136–144 (2015).

61. Li, Z. et al. Covalent triazine framework supported non-noble metal nanoparticles with superior activity for catalytic hydrolysis of ammonia borane: from mechanistic study to catalyst design. *Chemical Science.* **8** (1), 781–788 (2017).

Figure

Click here to access/download;Figure;Fig 1.tif

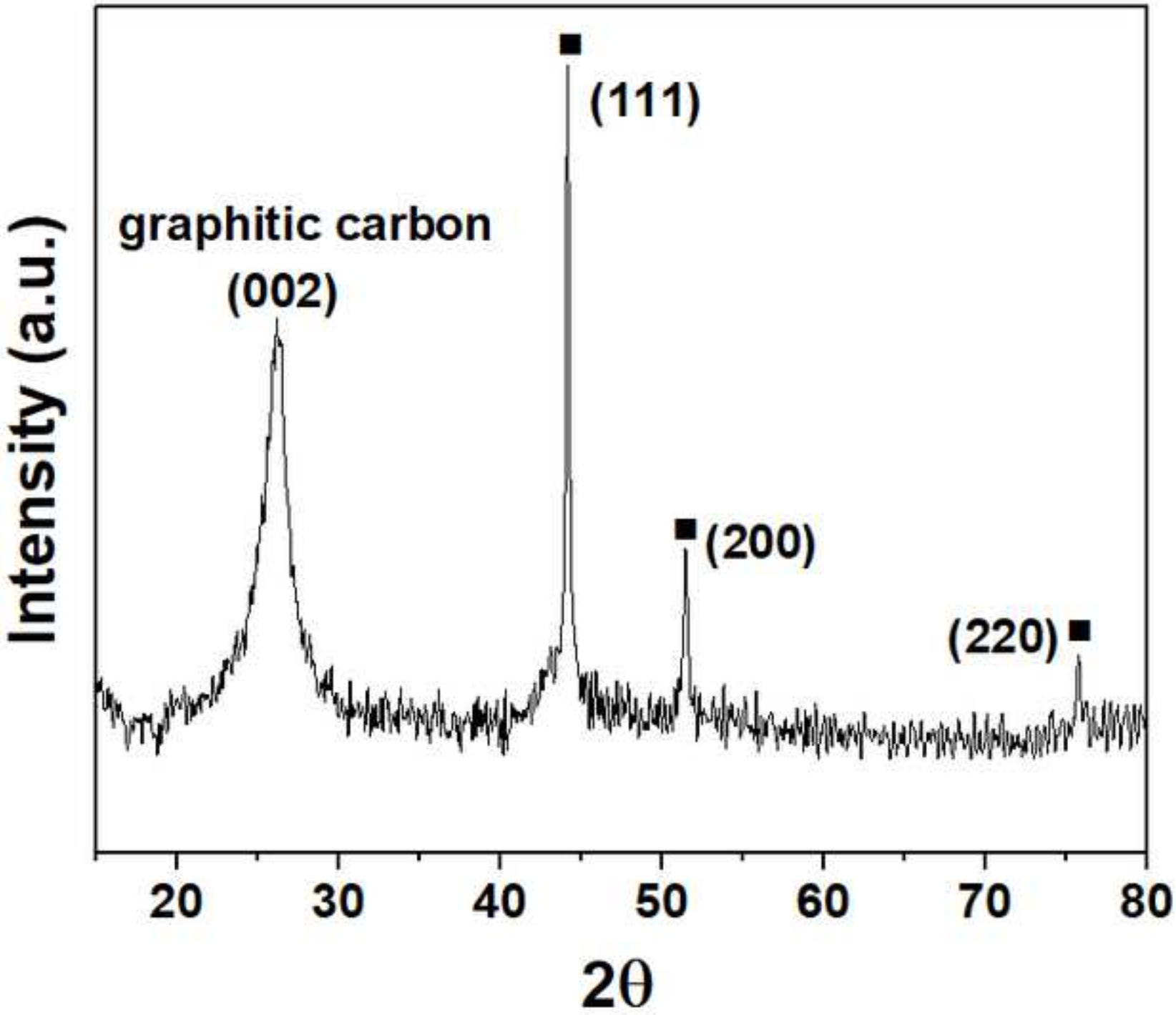

Figure

Click here to access/download;Figure;Fig 2.tif

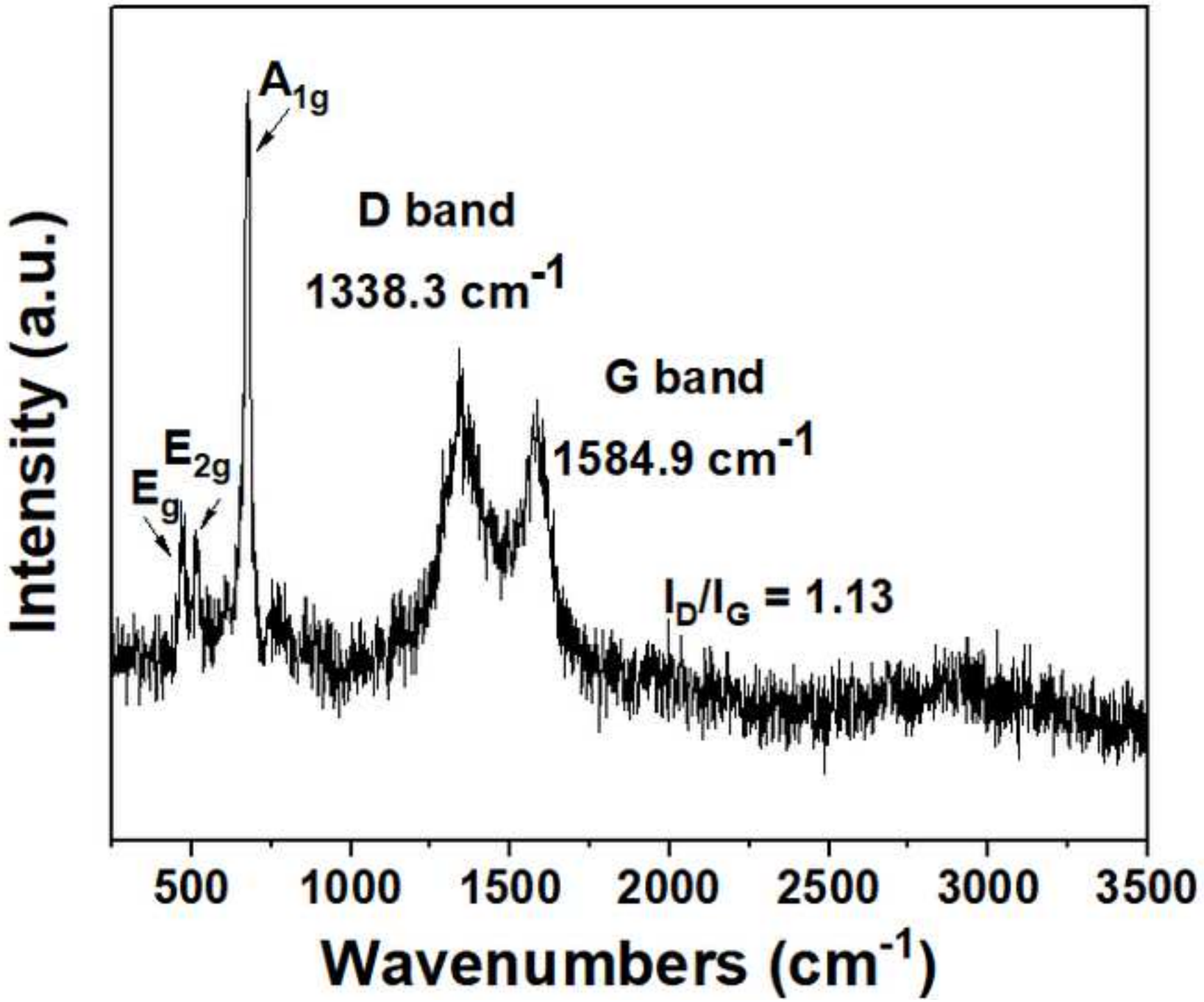

Figure

Click here to access/download;Figure;Fig 3.tif

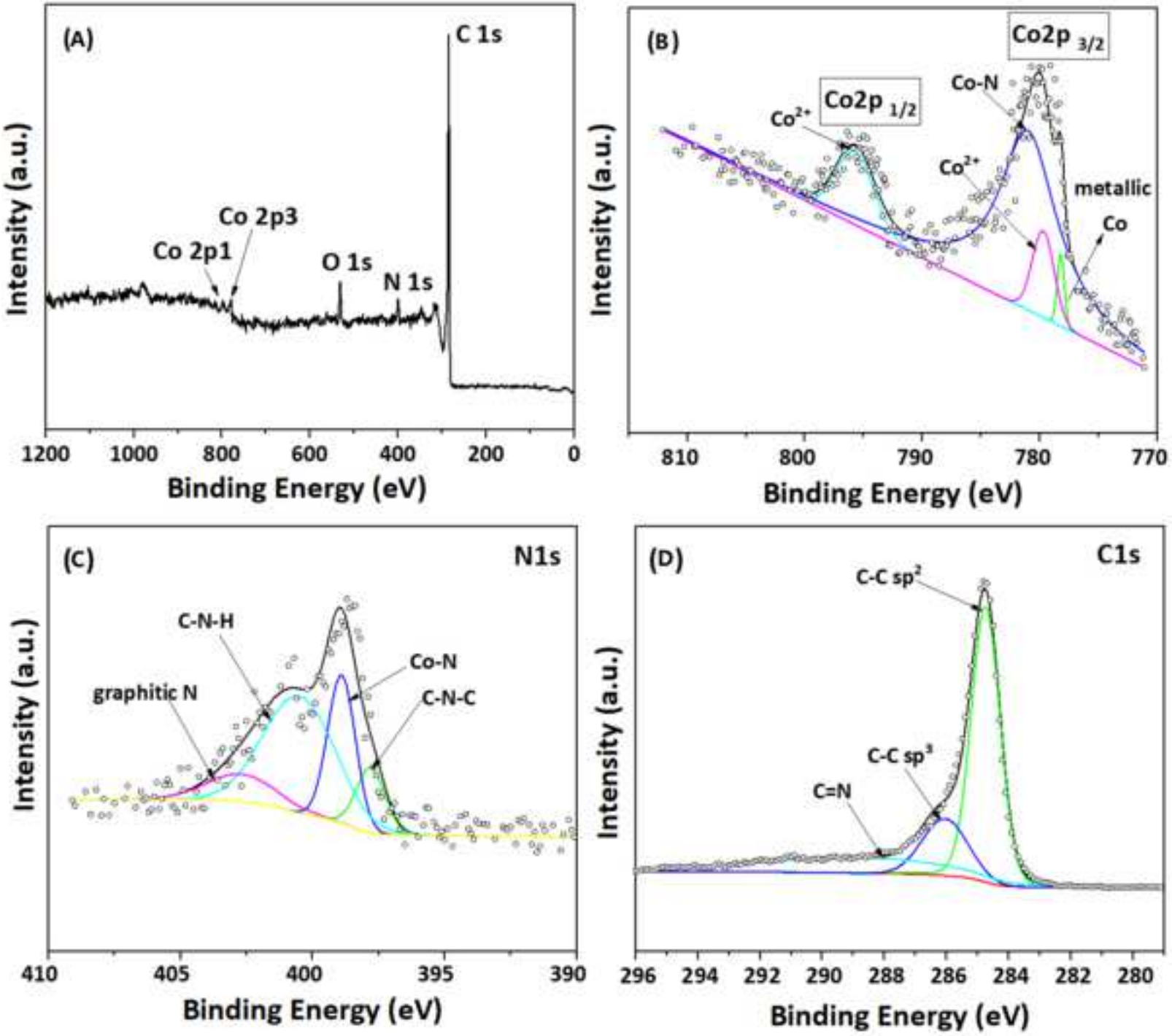

Figure

Click here to access/download;Figure;Fig 4.tif

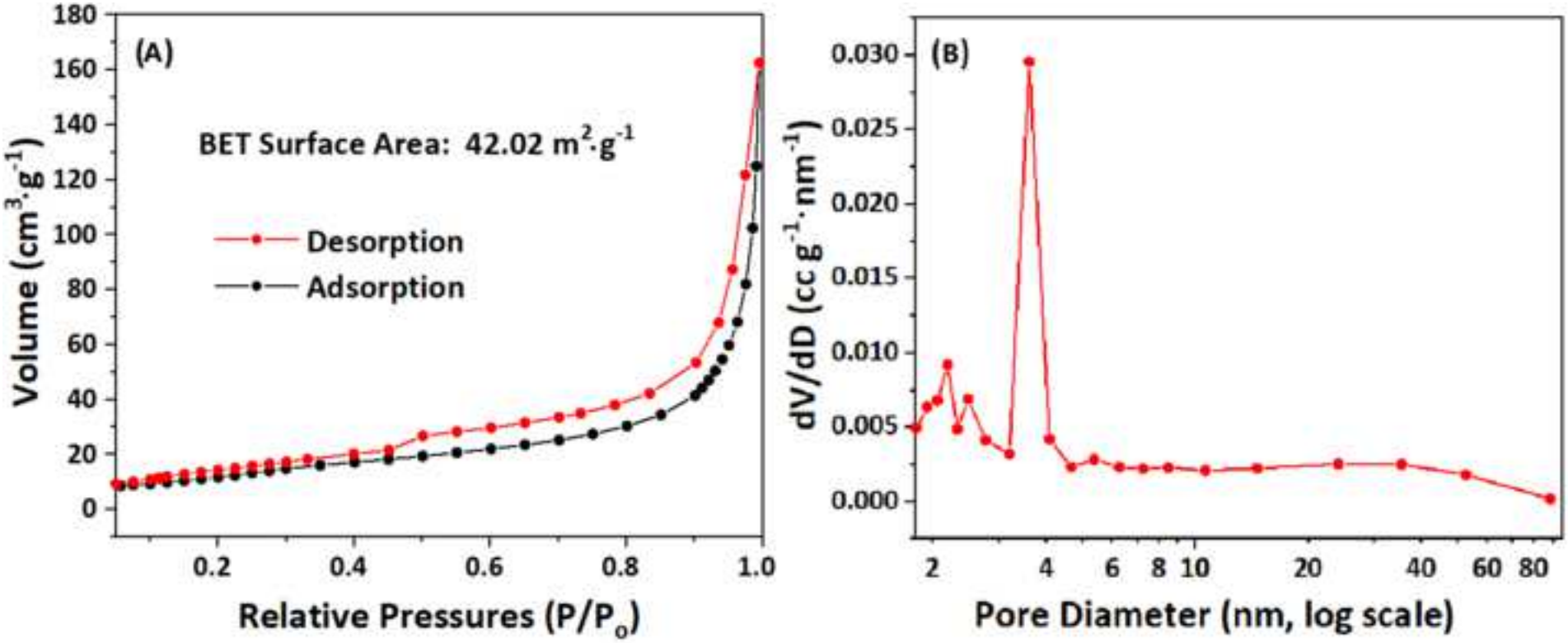

Figure

Click here to access/download;Figure;Fig 5.tif

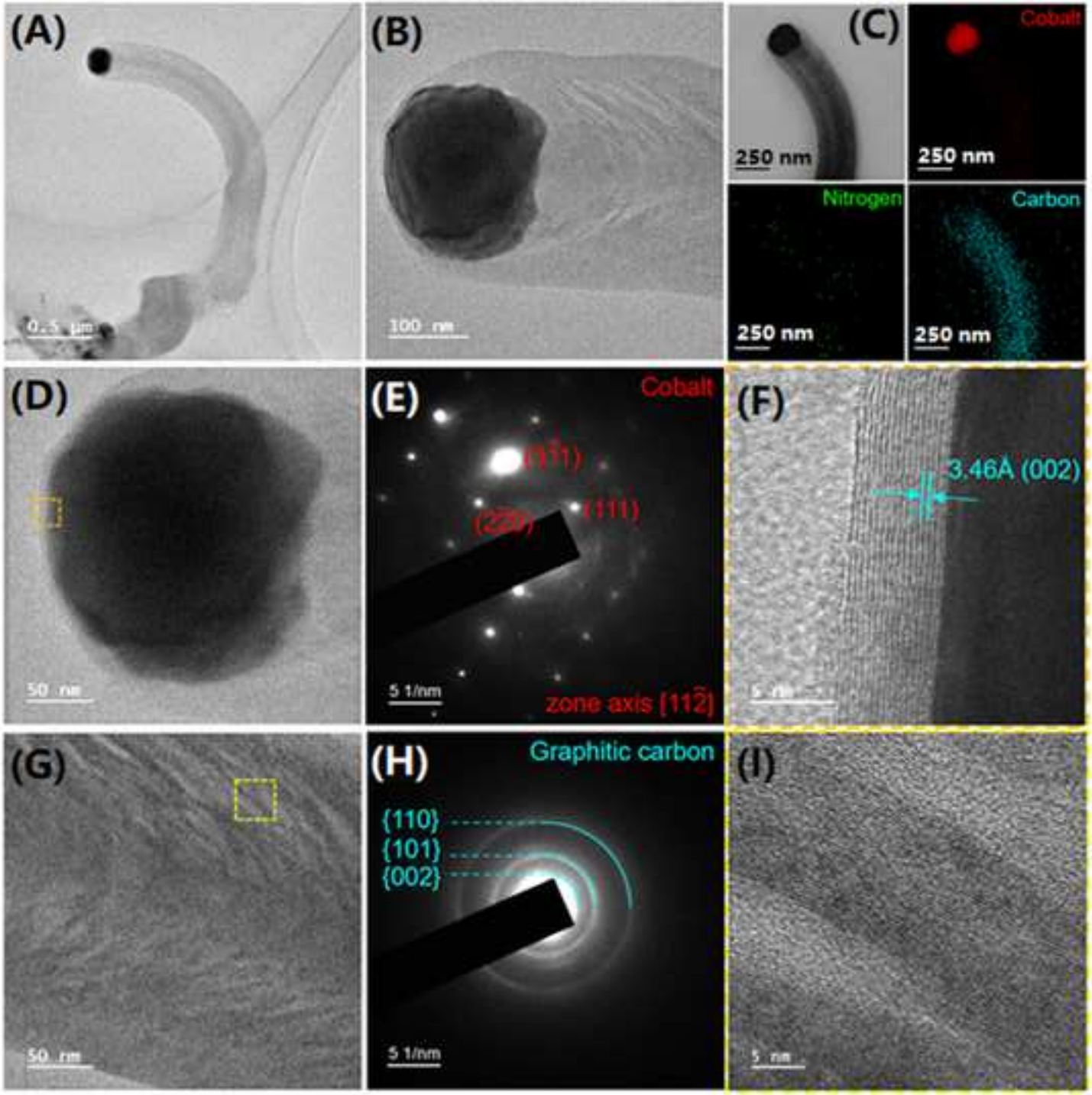

Figure

Click here to access/download;Figure;Fig.6.tif

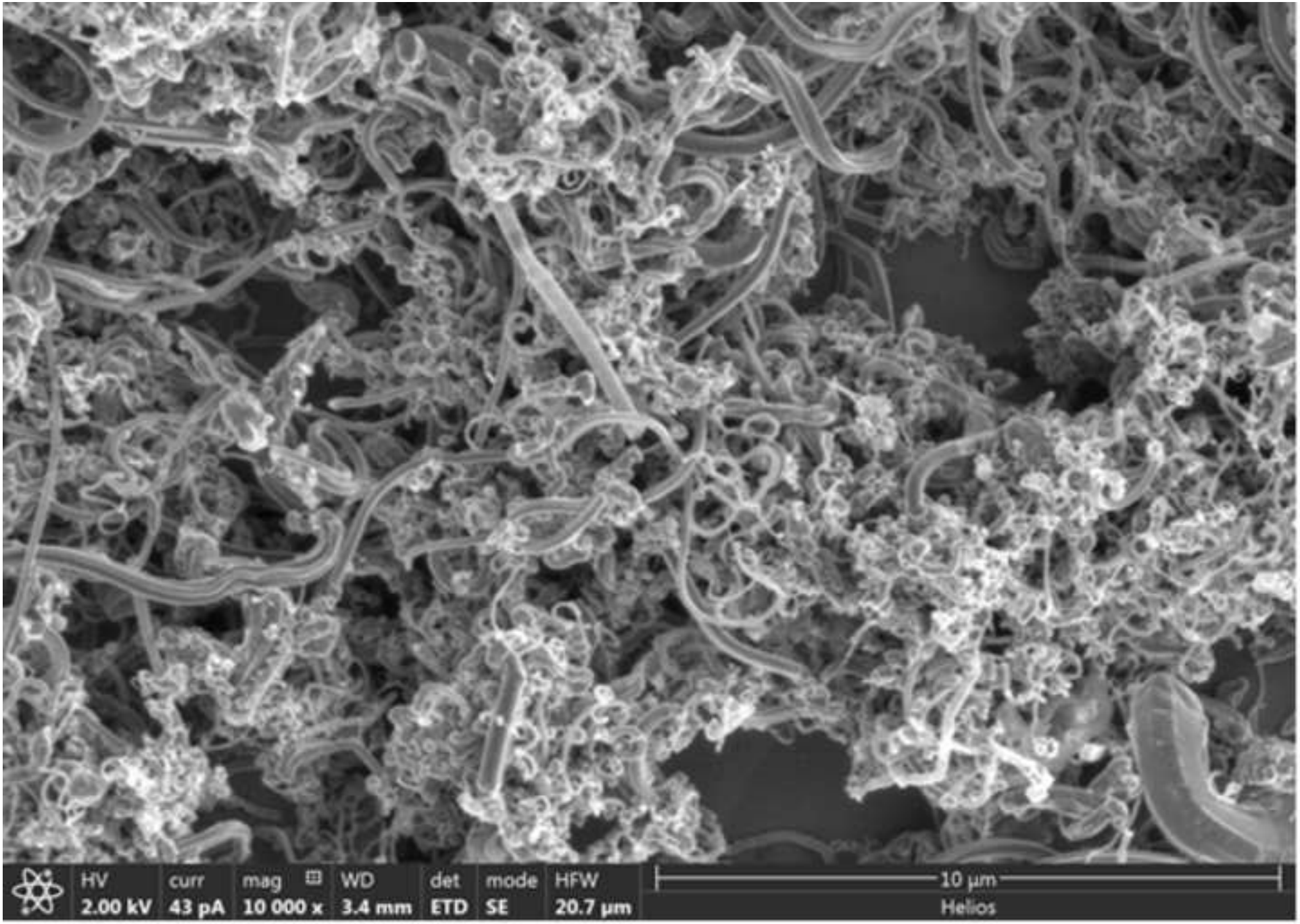

Figure

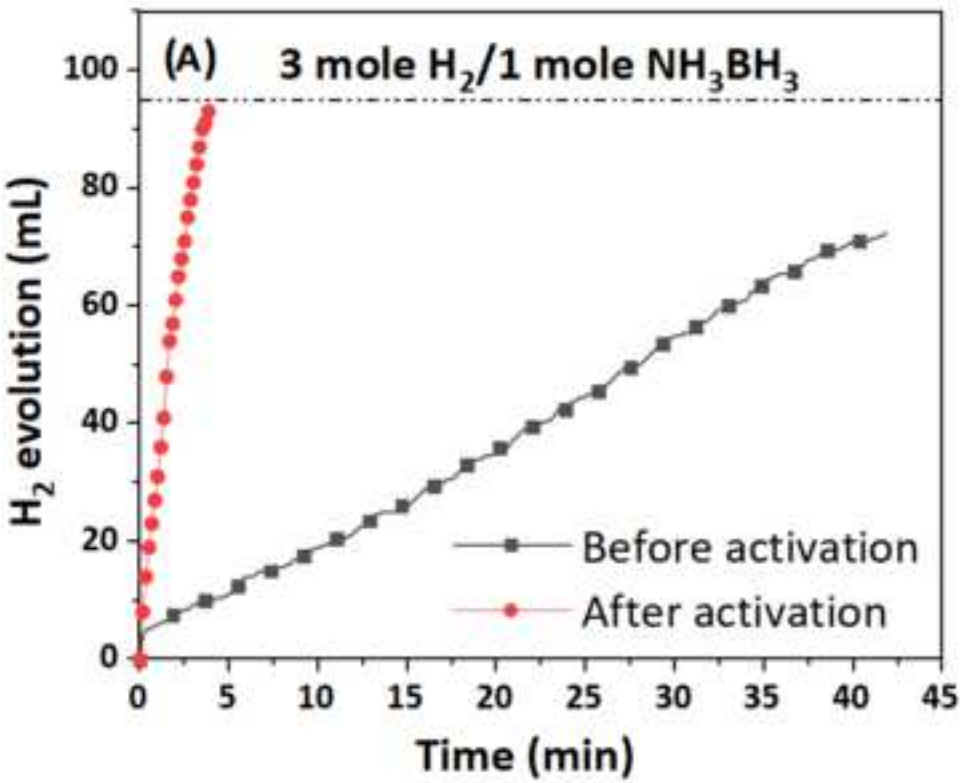

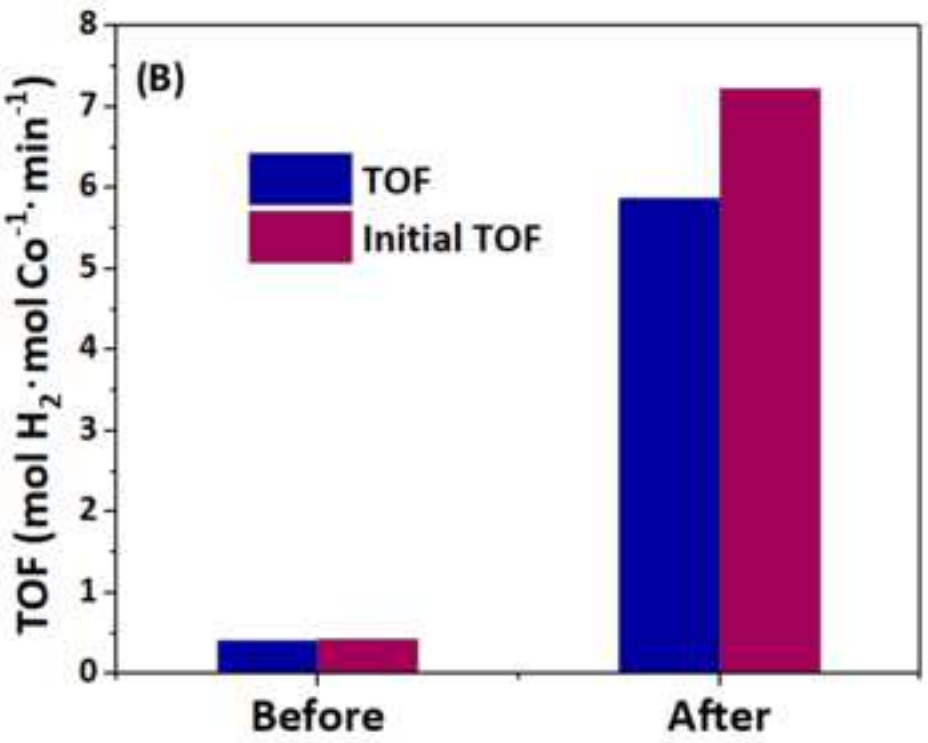

Figure

Click here to access/download;Figure;Fig 8.tif

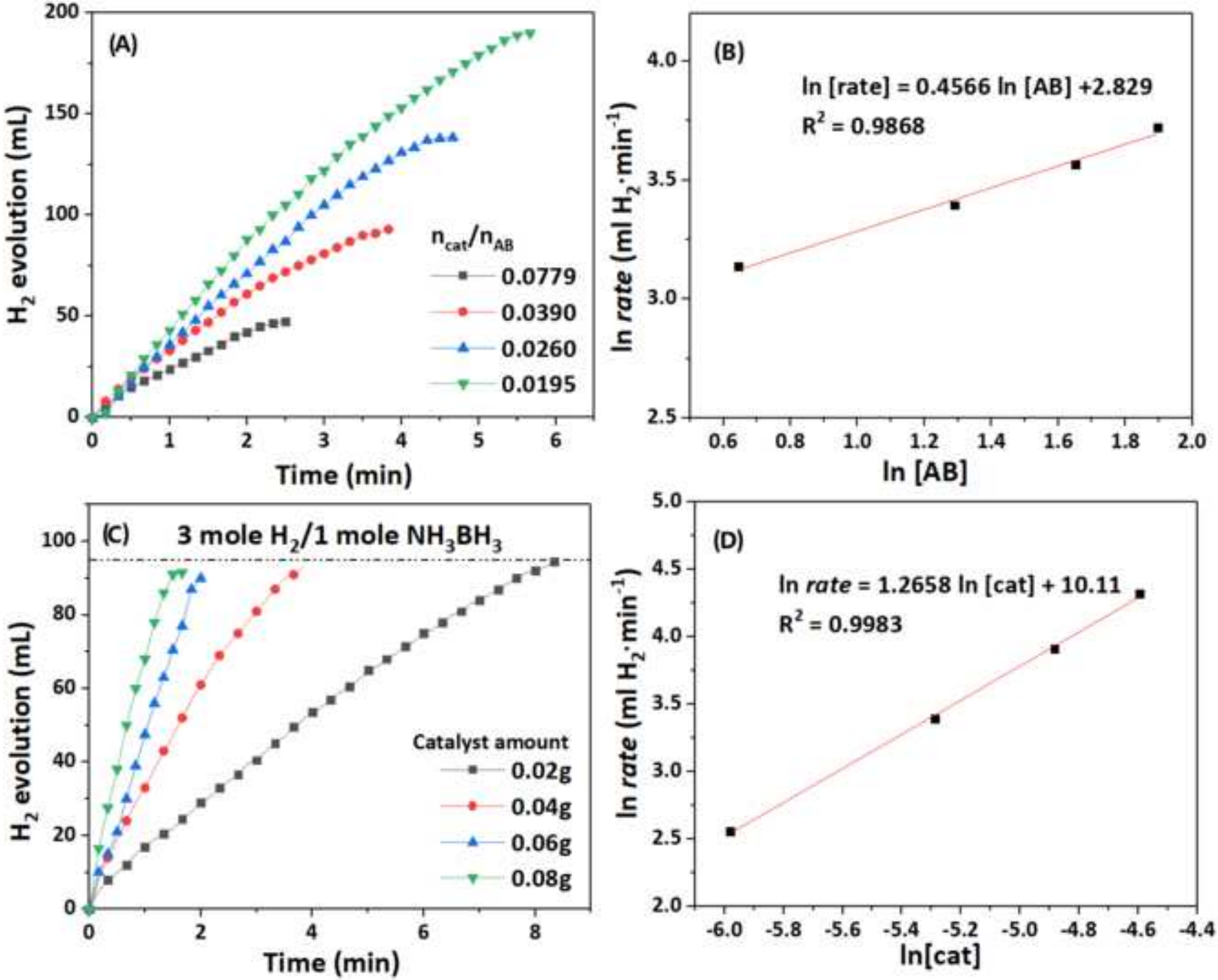

Figure

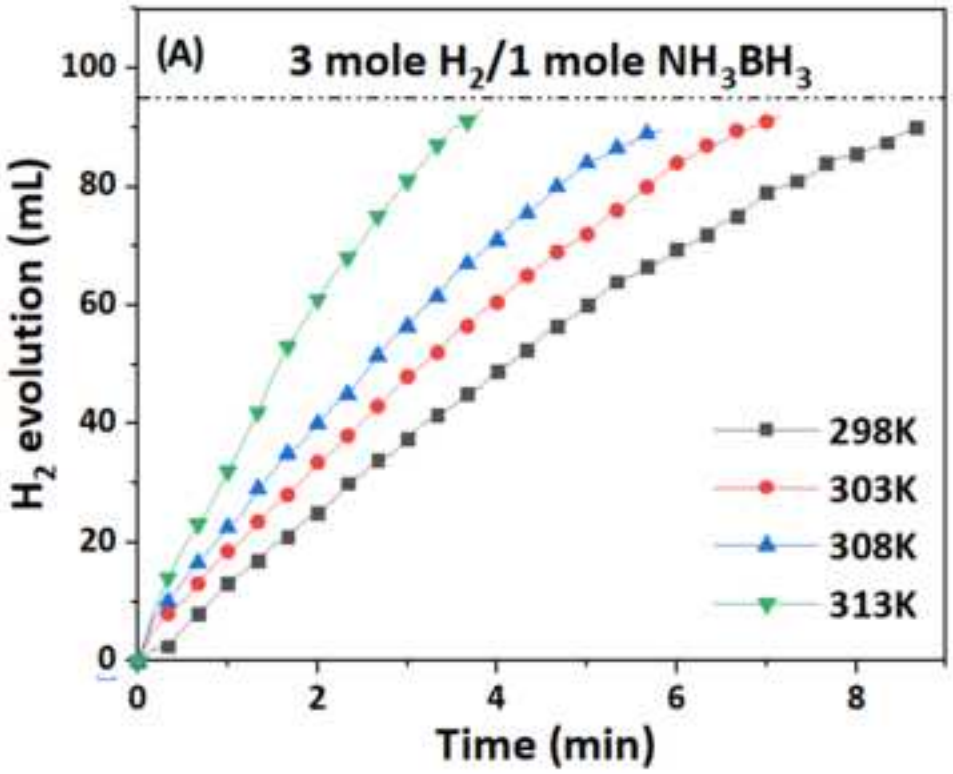

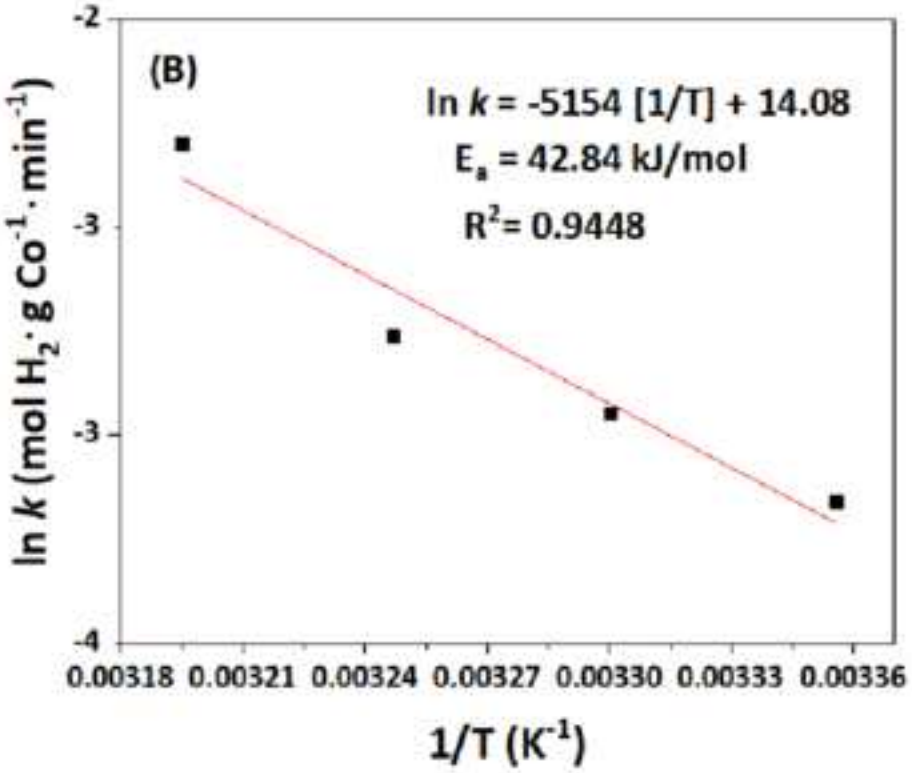

Figure

Click here to access/download;Figure;Fig 10.tif

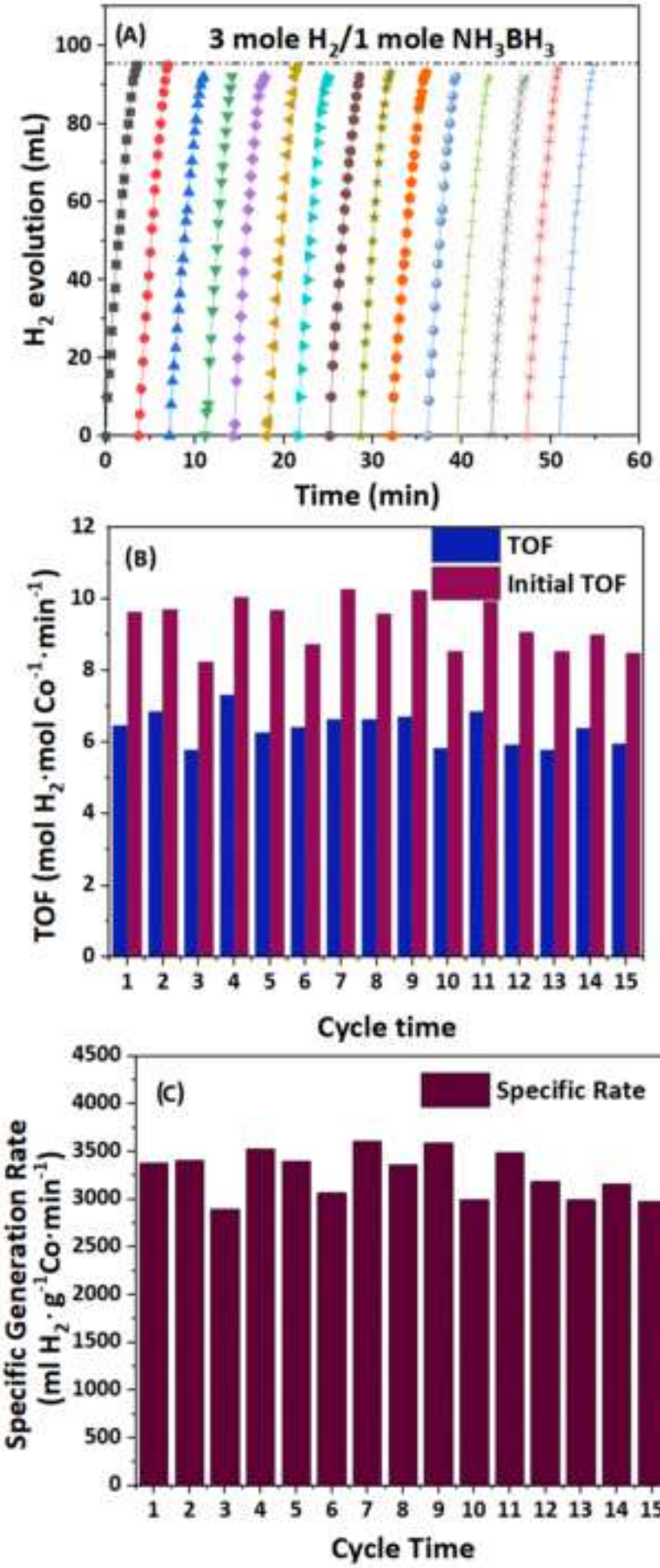

Figure

Click here to access/download;Figure;Figure 11.pdf

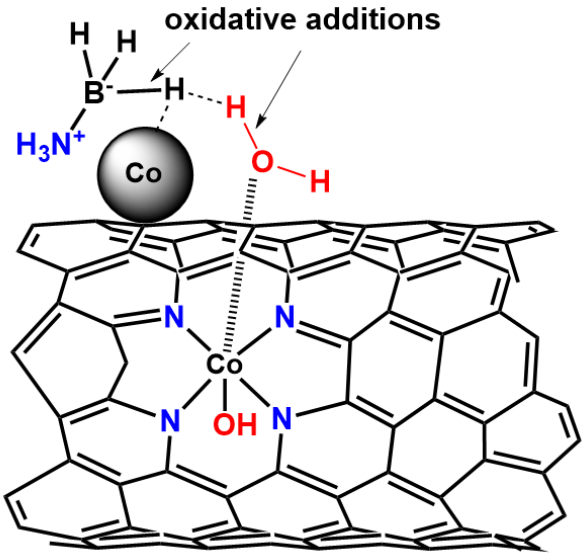

Table 1

Actual ICP-OES results	Total Co (wt%)	Co Nanoparticles (wt%)	Co Single Atoms (wt%)
0.5 wt% (nominal) Co/Co-N-CNT	25.1	9.7	15.4

Editorial comments:

Changes to be made by the Author(s):

1. Please take this opportunity to thoroughly proofread the manuscript to ensure that there are no spelling or grammar issues. Please define all abbreviations at first use.

Reply: Thanks for your reminding, we have checked all spelling and grammar issues, and the abbreviations are clarified.

2. Because one of your authors is from the UK, please sign the UK ALA.

Reply: Thanks for your reminding, we

3. Please revise the following lines to avoid overlap with previously published work: 293-294, 313-317, 323-325, 415-419, 421-422, 437-438.

Reply: Thanks for your checking, we have amended as follows:

Line 293-294

The broad peak at 2θ of 26.2° corresponds to the graphitic carbon (N-CNTs) indexed well to JCPDS card # 75-1621. Strong and sharp diffraction peaks indicate a well-defined crystalline structure. This is changed to:

The broad peak at 2θ of around 26° corresponding to the graphitic carbon (N-CNTs) can be indexed to JCPDS card # 75-1621. Well-defined crystalline structure are indicated by the strong and sharp diffraction peaks.

Line 313-317

The orbital peaks of the XPS survey spectrum divulge the presence of Co, N and C elements, as shown in **Figure 3a**. The high-resolution electron spectroscopy for chemical analysis (ESCA) of each element further reveals the chemical states of the elements. Three characteristics peaks are shown by spatial resolution of the Co $2p_{3/2}$ XPS profile in **Figure 3b**. This is changed to:

As shown in **Figure 3a**, the orbital peaks of the XPS survey spectrum signified the presence of N, C and Co elements. The high-resolution electron spectroscopy for chemical analysis (ESCA) of each element further indicates the chemical states of the elements. Three characteristics peaks, namely, the metallic Co, Co-N and Co^{2+}, are shown by spatial resolution of the Co $2p_{3/2}$ XPS profile as in **Figure 3b**.

Line 323-325

The ESCA spectrum of C1s can be deconvoluted into three main peaks, implying the different hybridization of carbon atoms during the formation of the nanotube structures. The peaks centered at 284.8, 286.1, 290.0 eV could be ascribed as C-C sp^3, C-C sp^2 and C=N respectively, as shown in Figure **3d**. This is changed to:

As shown in Figure **3d**, the ESCA spectrum of C1s can be resolved into three main peaks, indicating the different hybridization of carbon atoms during the formation of the carbon nanotube structures. The

peaks centered at around 285, 286 and 290 eV could be attributed to C-C sp^3, C-C sp^2 and C=N, respectively.

Line 415-419

Figure 8 Kinetics studies: (a) time plots of the catalytic dehydrogenation of AB at various AB concentration; (b) plot of H_2 generation rate vs. the concentration of AB both in natural logarithmic scale; (c) time plots of the catalytic dehydrogenation of AB with various catalytic amounts; (d) plot of H_2 generation rate vs. the concentration of catalyst both in natural logarithmic scale. This is changed to:

Figure 8 Kinetics studies: (a) time plots of the catalytic hydrolysis of AB versus AB concentration; (b) plot of H_2 generation rate versus AB concentration in natural logarithmic scale; (c) time plots of the catalytic hydrolysis of AB versus different catalyst amounts; (d) plot of H_2 generation rate versus the catalyst concentration in natural logarithmic scale.

Line 421-422

Figure 9 Kinetics studies: (a) time plots of the catalytic dehydrogenation of AB at various temperatures; (b) Arrhenius plots obtained from the kinetic data. This is changed to:

Figure 9 Kinetics studies: (a) time plots of the catalytic hydrolysis of AB at different temperatures; (b) Arrhenius plots obtained from (a).

Line 437-438

CoP NPs supported on N-CNT was obtained without any further treatment. The micropores acted as the pathway for Co and P precursors to permeate and coordinate to C and N atoms around the pores during pyrolysis process. This is changed to:

and the CoP NPs supported on N-CNT can be obtained. The presence of the micro-pores can act as the pathway for Co and P precursors to permeate during the pyrolysis and coordinate with the C and N atoms around the pores.

4. Please revise the text, especially in the protocol, to avoid the use of any personal pronouns (e.g., "we", "you", "our" etc.).

Reply: Thanks for your reminding, we have make the following amendment:

In line 44, A method for facile synthesis of nano-structured catalysts supported on carbon nanotubes with cobalt single atoms and nitrogen dopant is presented herein.

In line 104, Taking advantage of high N contents of the dicyandiamide and related C_3N_4 materials, a protocol for achieving facile synthesis of cobalt NPs supported on highly dispersed Co single atoms on N-doped carbon nanotubes is reported herein.

In line 110, Furthermore, Co/Co-N-CNT, as a result of the synergistic effects of strongly anchored Co NPs and the ability of the Co single atoms to lower the adsorption energy of water molecules, was successfully demonstrated. Thus realizing a superior stability in the hydrolysis of ammonia borane for hydrogen production.

In line 360, The presence of Co NPs was probably due to the high loading of metal precursor $Co(acac)_2$ used in the synthesis.

In line 443, In contrast, for Co SAs synthesis, it was found that as early as 700°C, Co NPs were already observed and it was found that pyrolysis at 800°C for 2 hours, 9.7 wt% of Co NPs were formed with about 15.4 wt% of Co SAs remaining.

5. Please ensure that all text in the protocol section is written in the imperative tense as if telling someone how to do the technique (e.g., "Do this," "Ensure that," etc.). The actions should be described in the imperative tense in complete sentences wherever possible. Avoid usage of phrases such as "could be," "should be," and "would be" throughout the Protocol. Any text that cannot be written in the imperative tense may be added as a "Note." However, notes should be concise and used sparingly. Please include all safety procedures and use of hoods, etc.

Reply: Thanks for your reminding, we have make the following amendment:

In line 117, Readers are advised to carefully check the properties and toxicities of the chemicals described in this paper for the proper chemicals handling fromrelevant material safety data sheets (MSDS). Some of the chemicals used are detrimental to health and special cares are to be taken. The impact of nanomaterials to human's health is unknown and may potentially pose safety hazards and health effects. Inhalation and skin contact should be avoided. Safety precaution shall also be exercised, such as releasing the waste gas during the catalyst synthesis to the fume hood and catalyst performance evaluation with proper venting of the hydrogen gas. Personal protective equipment is advised to be worn at all time. **Special Caution:** Hydrogen is a potentially explosive gas with a very broad flammability range from 4% to 74% in air. Care shall be taken to allow the hydrogen gas to vent properly to the atmosphere.

6. 4.1.8.—Don't highlight equations.

Reply: We have removed the equation highlight in line 179.

7. Please note that your protocol will be used to generate the script for the video and must contain everything that you would like shown in the video. Please ensure you answer the "how" question, i.e., how is the step performed? Alternatively, add references to published material specifying how to perform the protocol action. There should be enough detail in each step to supplement the actions seen in the video so that viewers can easily replicate the protocol.

Reply: Thanks for your reminding, we will ensure the video script will be written in the style of how to perform each steps.

8. Please format the manuscript as: paragraph Indentation: 0 for both left and right and special: none, Line spacings: single. Please include a single line space between each step, substep and note in the protocol section. Please use Calibri 12 points and one-inch margins on all the side. Please include a ONE LINE SPACE between each protocol step and then HIGHLIGHT up to 3 pages of protocol text for inclusion in the protocol section of the video.

Reply: We have amended the line spacing type to be single line for the whole manuscript. We have also included a single line space between each step and sub-step.

9. As there is overlap in your legends with other literature sources, please obtain explicit copyright permission to reuse any figures from a previous publication. Explicit permission can be expressed in the form of a letter from the editor or a link to the editorial policy that allows re-prints. Please upload this information as a .doc or .docx file to your Editorial Manager account. The Figure must be cited appropriately in the Figure Legend, i.e. “This figure has been modified from [citation].”

Reply: Thanks for your reminding, we confirmed that all figures and tables have never been published elsewhere.

10. Please combine all panels of one figure into a single image file.

Reply: Thanks for your reminding, we have re-arrange the following panels of figures into single TIFF image files:

Figure 3, Figure 4, Figure 7, Figure 8, Figure 9 and Figure 10.

11. Please include a scale bar for all images taken with a microscope to provide context to the magnification used. Define the scale in the appropriate Figure Legend.

Reply: Thanks for your reminding, we have added scale bar to Figure 6.

Reviewers' comments:

Reviewer #1:

Manuscript Summary:

Lee et al. have reported the synthesis of metal nanoparticles supported on carbon nanotube with doped Co and N atoms and its catalytic applications in hydrogen production from ammonia borane solution. The manuscript is well organized, I will recommend its publication in Journal of Visualized Experiments after minor revisions.

Reply: Thanks for the comments. The concerns are addressed as follows:

Major Concerns:

Based on the XPS results, the authors claim there are single atoms of Co in their sample. Please provide powerful proof for this, otherwise, please revise this statement.

Reply: Change was made in line 321: The relatively stronger peak at 397.8 eV could be attributed to the presence of the strong interaction of metallic cobalt with nitrogen atoms [19,21], which could be either cobalt nanoparticles or/and cobalt single atoms.

Minor Concerns:

1. Generally speaking, the hydrolysis is a zero-order reaction with respect to ammonia borane. But the result in this work is quite different, please explain this.

Reply: Thanks for the comment. This is due to the slight induction period of AB activation on the catalyst surface. In fact, addition of alkaline ion fastens the reaction, just like most other results reported in the literature. Thus, in line 370, we amended the statement as: The rate showed a slight dependence on ammonia borane and reaction order of the catalyst was about 0.4, which was quite different from most other reported rate law in the hydrolysis of ammonia borane, but is similar to the one reported on the AB hydrolysis by CoP nanoparticles, which was reported as 0.6 due to the longer induction time of AB on the catalyst [25].

2. Can you provides the XRD pattern of the catalyst after 15 catalytic cycles?

Reply: Thanks for the comments. We have repeated the reaction and analyze the XRD pattern of the catalysts after 15 times of reaction run. It showed that there is no observable changes compared with the original samples before run.

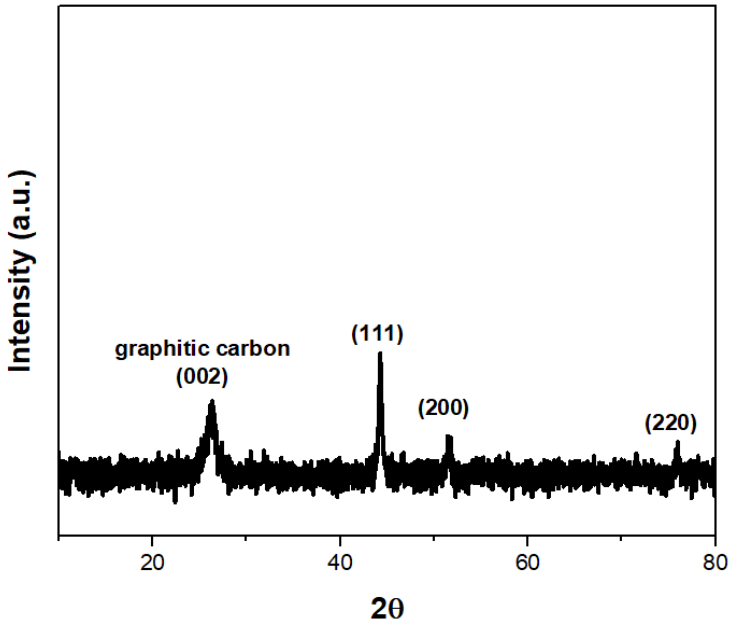

3. Some recent publications related to ammonia borane hydrolysis may help the readers to understand this work well and please cite them. Renewable Energy 2021, 169: 660-669; ACS Applied Energy Materials 2021, 4: 633-642; International Journal of Hydrogen Energy 2020, 45: 8168-8176; Small 2019, 15, 1805460.

Reply: Thanks for the suggestion. The following texts have been added to the introduction part of the manuscript:

Recently, catalysts with hollow micro/nanostructures have been exploited for AB hydrolysis. These materials are conventionally prepared by hydrothermal methods and have been widely used for lithium-ion batteries, supercapacitors, chemical sensor and heterogeneous catalysis research. Thus, the copper-cobalt synergy towards AB hydrolysis has been demonstrated by the hollow $CuMoO_4$-$CoMoO_4$ [25], which give a high TOF of 104.7 min^{-1}. Other highly structural-dependent examples such as the core-shell CuO-NiO/Co_3O_4 [26], the $Co_xCu_{1-x}Co_2O_4$@$Co_yCu_{1-y}Co_2O_4$ yolk-shell type [27] and the $Ni_{0.4}Cu_{0.6}Co_2O_4$ nanoarrays [28] were also found to be active towards AB hydrolysis.

Reviewer #2:

Manuscript summary:

Authors have reported synthesis of metal nanoparticles supported on carbon nanotubes with doped N atoms and its catalytic applications in hydrogen production. This manuscript includes a protocol to prepare Co nanoparticles on N-doped carbon nanotubes. The protocol provides the synthesis of materials, experimental methods, and analysis methods. This work is useful to show from the beginning to the end of the project for hydrogen production. However, some points need to be clarified and discussed.

Reply: Thanks

Comments to the Authors:

1. The authors need to provide some information about various methods for hydrogen production in Introduction.

Reply: Thanks. The following texts have been added to the introduction:

In the past few decades, hydrogen has been regarded as a potential alternative to replace fossil fuels or hydrocarbons, such as coal, natural gas and gasoline due to the advantage of zero-emission of the former. Until now, about 94% of commercial hydrogen is still produced from the reforming process of fossil fuels, in which the process release a great deal of greenhouse gas [14]. Therefore, hydrogen production from renewable resources such as water electrolysis is a way to solve the problem of depleted fossil resources and severe carbon emission. However, the low hydrogen production efficiency has hindered their wider applications. Thus, to overcome this kinetic energy barriers for water-splitting, numerous efficient electro-catalysts have been discovered in the past decade [15]. Another issue is the storage problem due to the gaseous and explosive nature of hydrogen gas at ambient conditions. Physical storage methods such as compression will require the hydrogen to be compressed up to 700-800 bar and cryogenic storage by liquefaction will require low temperature at -253°C [16].

2. The authors need to provide some information about various materials for hydrogen production in Introduction.

Reply: Thanks. The following texts have been added to the introduction:

Although commercialized hydrogen fuel cell-powered vehicles have been successfully demonstrated, the storage problem is yet to be solved if the technology is to be used in wider applications, such as miniature devices and mini-fuel cells. Thus, storage methods of using chemical H materials have been one of the hot focus in hydrogen energy research. Some examples of chemical H storage materials are ammonia borane (AB) [17], formic acid (FA) [18], ammonia gas [19], sodium alanate [20] and magnesium hydride [21]. Among these, AB has a low molecular weight (30.7 g/mol), high gravimetric and volumetric densities (196 gH_2 kg^{-1} and 146 gH_2 L^{-1}, respectively). Besides, it is an air and moisture stable compound, non-toxic and highly soluble in water. Metal nanoparticles on various supported materials have been widely used to release the three equivalents of hydrogen from AB, such as platinum- (Pt-), palladium- (Pd-), ruthenium- (Ru-), cobalt- (Co-) and nickel- (Ni-) based catalysts. Co-based heterogeneous catalysts supported on carbon materials are especially attracting much attentions due to their low cost, high abundancy and ease of recovery. Several

synthetic strategies have been reported such as the Co NPs supported on branched polyethylenimine-decorated graphene oxide [22]. The 3D structure with large surface area ensure the stabilization of Co NPs maintaining at the 2-3 nm size range and prevented the aggregation of NPs. Another strategy is to use N-doped carbon materials to support Co NPs with small sizes. Using Co(salen) [23] and Co-MOF [24] (metal organic framework) as the precursors, Co NPs of 9.0 nm and 3.5 nm supported on N-doped porous carbon materials have been prepared respectively. The stability towards AB hydrolysis are high and the reactivity can maintain over 95% of the initial activity after 10 reaction runs. Recently, catalysts with hollow micro/nanostructures have been exploited for AB hydrolysis. These materials are conventionally prepared by hydrothermal methods and have been widely used for lithium-ion batteries, supercapacitors, chemical sensor and heterogeneous catalysis research. Thus, the copper-cobalt synergy towards AB hydrolysis has been demonstrated by the hollow $CuMoO_4$-$CoMoO_4$ [25], which give a high TOF of 104.7 min^{-1}. Other highly structural-dependent examples such as the core-shell CuO-NiO/Co_3O_4 [26], the $Co_xCu_{1-x}Co_2O_4$@$Co_yCu_{1-y}Co_2O_4$ yolk-shell type [27] and the $Ni_{0.4}Cu_{0.6}Co_2O_4$ nanoarrays [28] were also found to be active towards AB hydrolysis. Maximizing the interaction between the catalysts and substrates is also another strategy for AB hydrolysis. Chiang et al. have utilized the surface oxide group of graphene oxide to form an initiated complex species with AB [29], thus $Ni_{0.8}Pt_{0.2}$/GO and rGO demonstrated excellent reactivity towards AB hydrolysis. The use of α-MoC as support for Co and Ni single atom catalysts assisted the activation of water molecules and achieved high TOF towards AB hydrolysis, which is four times higher than the commercial Pt/C catalyst [30].

3. The quality of figures needs to be improved. Some fonts and labels are too small or not clear.

Reply: Thanks.

We have modified the scale bar of Figure 5 and enlarged the fonts and the labels in other all other figures..

4. Advanced and potential materials have been developed for the field. Thus, the authors should add the information in Introduction from the following references: Chemical Society Reviews, 50, 6700-6719, 2021, https://doi.org/10.1002/adma.202008422, Chemical Society Reviews, 50, 1354-1390, 2021, Advanced Energy Materials, 11, 2100157, 2021, Journal of Materials Chemistry A, 9, 2999-3006, 2021, Advanced Functional Materials, 30, 1910768, 2020, Matter, 2, 526-553, 2020, Journal of Materials Chemistry A, 8, 10604-10624, 2020, Journal of Materials Chemistry A, 8, 7109-7116, 2020, Journal of the American Chemical Society, 141, 18578-18584, 2019, Small, 16, 2002426, 2020

Reply: Thanks for the suggestion. We found that these types of heterostructured catalysts could be potentially useful in the hydrogen evolution reaction from chemical H storage materials. Thus, we have selected the following literatures and cite them in the introduction part.

Jose, V. *et al.* Highly Efficient Oxygen Reduction Reaction Activity of N-Doped Carbon–Cobalt Boride Heterointerfaces. *Advanced Energy Materials.* **11** (17), doi:10.1002/aenm.202100157, (2021).

Li, M. *et al.* Gd-induced electronic structure engineering of a NiFe-layered double hydroxide for efficient oxygen evolution. *Journal of Materials Chemistry A.* **9** (5), 2999-3006, doi:10.1039/d0ta10740a, (2021).

Lin, Y. *et al.* Co-Induced Electronic Optimization of Hierarchical NiFe LDH for Oxygen Evolution. *Small.* **16** (38), e2002426, doi:10.1002/smll.202002426, (2020).

Prabhu, P., Jose, V. & Lee, J. M. Heterostructured Catalysts for Electrocatalytic and Photocatalytic Carbon Dioxide Reduction. *Advanced Functional Materials.* **30** (24), doi:10.1002/adfm.201910768, (2020).

Prabhu, P. & Lee, J. M. Metallenes as functional materials in electrocatalysis. *Chem Soc Rev.* **50** (12), 6700-6719, doi:10.1039/d0cs01041c, (2021).

Wang, H. *et al.* Electronic Modulation of Non-van der Waals 2D Electrocatalysts for Efficient Energy Conversion. *Adv Mater.* **33** (26), e2008422, doi:10.1002/adma.202008422, (2021).

Wang, H. & Lee, J.-M. Recent advances in structural engineering of MXene electrocatalysts. *Journal of Materials Chemistry A.* **8** (21), 10604-10624, doi:10.1039/d0ta03271a, (2020).

Qiu, X. *et al.* Hydrogen generation from ammonia borane hydrolysis catalyzed by ruthenium nanoparticles supported on Co–Ni layered double oxides. *Sustainable Energy & Fuels.* **5** (8), 2301-2312, doi:10.1039/d1se00079a, (2021).

And in the manuscript, we have added the following:

Another type of emerging materials known as the heterostructured catalysts such as MXenes and layered double hydroxides (LDHs) are increasingly being exploited for electrocatalytic and photocatalytic reaction [29-32]. These materials such as the NiFe-layered double hydroxide [33,34] and the CoB-N materials having N-doped carbon-cobalt boride heterointerfaces [35] are especially active for oxygen evolution and reduction reaction. In principles, they could be further exploited for hydrogen evolution reaction from hydrogen storage materials such as ammonia borane [36].

5. Typos and errors should be corrected in the whole manuscript.

Reply: Thanks, we have checked the typos and errors of the whole manuscript again.

Reviewer #3:

Manuscript Summary:

In this work, authors proposed the heterogeneous catalyst composed of both Co nanoparticles and Co single atoms supported on N-doped carbon nanotubes, which showed excellent activity and stability towards the hydrolysis reaction of ammonia borane for hydrogen gas production. The authors provided some reasonable explanations on the results they obtained. Therefore, the reviewer approves its acceptance for publication with minor revisions.

Reply: Thanks

Minor Concerns:

(1)In Raman spectrum, the D band (1358 cm-1) and G band (1580 cm-1) are not consistent with Figure 2.

Reply: We are sorry for the careless mistakes. We have amended the value in the manuscript, thus, in line 300:

The D band, which was attributed to the structural deformation of the sp^3-hybrizied carbon vibrations, can be assigned to the peak at 1338 cm^{-1}. The G band, which was due to the E_{2g} scattering vibrational mode of first-ordered scattering in a hexagonal lattice by the sp^2-hybridized carbon domain, can be assigned to the peak at 1585 cm^{-1}.

(2)"The main body of the carbon nanofiber was endowed with amorphous and porous structure." Note that the porous structure is ambiguous from Figures 5g-i, please check it carefully.

Reply: Thank you for the comment. The sentence has been revised to “The main body of the carbon nanofiber is endowed with graphitic carbon layers of different orientations, as shown in Figures 5g and 5i”.

The below Figure (a) shows the graphitic carbon layers around the Co nanoparticle from the fiber tip (left) to the main body of carbon nanofiber (right), and the below Figure (b) shows the different orientations of the graphitic carbon layers in the main body of the carbon nanofiber.

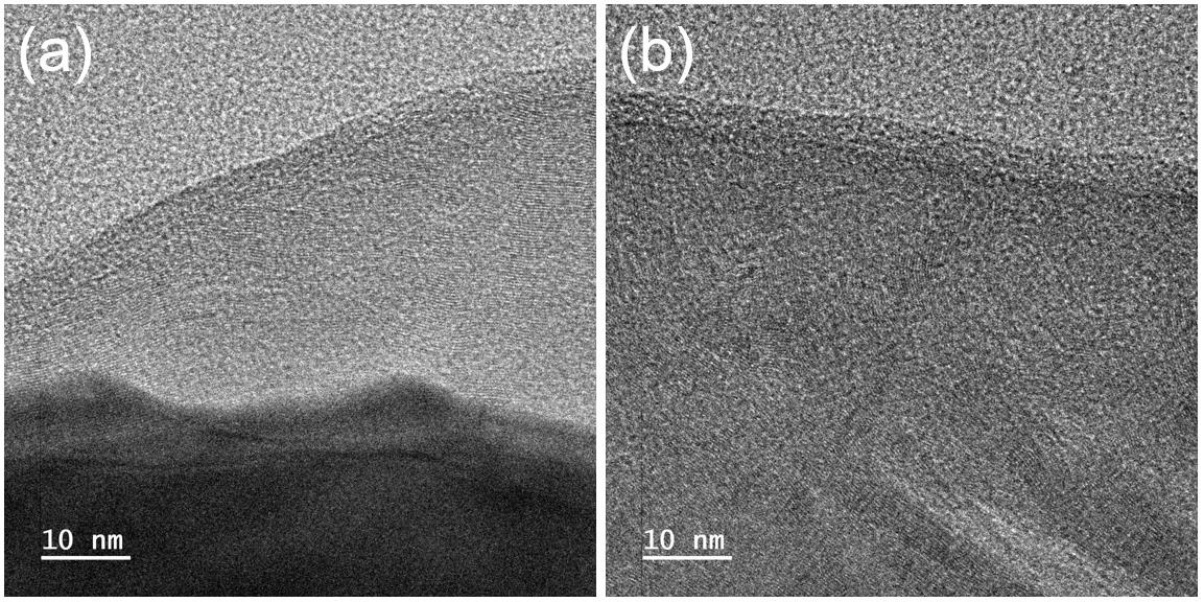

(3)It is suggested to provide ICP-OES experimental results in figure or table.
The description of Figure 10 in the manuscript is inconsistent with the annotations of figures, please check it carefully.

Reply: Thanks for the reminder. The table was listed in the manuscript as Table 1 at line 361:

Actual ICP-OES results	Total Co (wt%)	Co Nanoparticles (wt%)	Co Single Atoms (wt%)
0.5 wt% (nominal) Co/Co-N-CNT	25.1	9.7	15.4

For the inconsistent annotations, we have corrected as follows:

In line 424,

Figure 10 (a) Recycling of 0.5 wt % Co/Co SACs catalyst (40 mg) in water (10 mL), with addition of AB (1.30 mmol) to the system at 313 K in each cycle. (b) the TOF ratio at each recycles. (c) the specific generation rate.

Reviewer #4:

Manuscript summary:

In this paper, a heterogeneous catalyst supported by Co NPs and Co SAs on carbon nanotube (CNT) nanostructure has been demonstrated to have good catalytic activity. At the same time, the results showed that the prepared nanocatalysts had abundant active sites and high defect density. The excellent synergistic effect of NPS and SAs was proved. But there are many inconsistencies in the paper and many holes in the research results. I hope the author can review and think again.

Reply: Thanks, the following concerns are addressed as follows:

1. According to Fig. 5d and Fig. 5f, the Co nanoparticles are coated by several layers of graphite carbon. How does cobalt play its most effective role?

Reply: Thanks for the comments.

Although the Co nanoparticles are covered by several layers of graphitic carbons, this does not affect the reactivity substantially due to high defect intensity, high specific surface area and high pore volume.

According to the Raman spectrum, there are surface defects of the catalysts caused by nitridation by the partial NH_3 atmosphere, which may be used to explain the presence of active sites for the hydrolysis reaction. The intensities of the D band to G band (I_D/I_G) is 1.13, which is in the high range and is widely believed to favor increasing the number of active sites for many catalytic reaction such as electrocatalytic water splitting. (Ref: Fei, H. *et al.* Atomic cobalt on nitrogen-doped graphene for hydrogen generation. *Nat Commun.* **6** 8668, doi:10.1038/ncomms9668, (2015).)

Porosity is another factor. Porous carbons are characterized by their highly developed micro- and meso-pore structures. The high porosity and large surface area facilitate the access of active sites and the mass transport of AB and hydrogen. (Ref: Li, Y.-T., Zhang, X.-L., Peng, Z.-K., Liu, P. & Zheng, X.-C. Hierarchical Porous g-C_3N_4 Coupled Ultrafine RuNi Alloys as Extremely Active Catalysts for the Hydrolytic Dehydrogenation of Ammonia Borane. *ACS Sustainable Chemistry & Engineering.* **8** (22), 8458-8468, doi:10.1021/acssuschemeng.0c03009, (2020).) The present materials with BET surface area: 42.02 $m^2\ g^{-1}$ and Pore volume 0.25 $cm^3\ g^{-1}$ is comparable to the reported $Ru_{0.5}Ni_{0.5}$/p-g-C_3N_4 catalysts (BET surface area: 43.2 $m^2\ g^{-1}$ and Pore volume 0.28 $cm^3\ g^{-1}$) which is also excellent catalyst towards the AB hydrolysis reaction. (Ref: Li, Y.-T., Zhang, X.-L., Peng, Z.-K., Liu, P. & Zheng, X.-C. Hierarchical Porous g-C3N4 Coupled Ultrafine RuNi Alloys as Extremely Active Catalysts for the Hydrolytic Dehydrogenation of Ammonia Borane. *ACS Sustainable Chemistry & Engineering.* **8** (22), 8458-8468, doi:10.1021/acssuschemeng.0c03009, (2020).)

In contrast to the traditional view that the transition-metal such as Co nanoparticles embedded in a few-layer graphitic shells would be catalytically inert, they may show higher activities toward some catalytic reaction such as electrocatalysis reactions (ORR, OER and HER). On one hand, the metal nanoparticles not only catalyze the formation of hollow carbon structures such as carbon nanotubes, which could improve electrical conductivity of the whole hybrid structures. On the other hand, the few-layer graphitic shells could prevent the embedded metal nanoparticles from the acid corroding, oxidizing and aggregating during the catalysis processes, resulting in the excellent durability and stability in tough environments. Moreover, the cobalt nanoaprticle@N-doped carbon nanotube may provide an effective pathway to tailor the electronic structure of the catalyst, and thereby greatly decreases the adsorption free energy of the

AB substrate, which would promote the adsorption and desorption of reaction intermediates. (Ref: Guo, H. *et al.* Cobalt nanoparticle-embedded nitrogen-doped carbon/carbon nanotube frameworks derived from a metal–organic framework for tri-functional ORR, OER and HER electrocatalysis. *Journal of Materials Chemistry A.* **7** (8), 3664-3672, doi:10.1039/c8ta11400e, (2019).) Although the current system may not be the best for optimal reactivity, the optimal number of graphitic layers in the current catalytic system for AB hydrolysis is currently still underway.

2. Is the defect due to the addition of cobalt or due to nitriding? It's not explained in the manuscript.

Reply: Thanks for the comment. To verify that the defect was caused by the NH_3 atmosphere, we have also performed carbonization reaction with lesser amount of DCD-350 (higher wt% of Co). With 3wt% Co precursor (1:33.3), the Raman spectrum show a significant decrease of (ID/IG), which is 0.6. Also, CoN_4 was not observed for the 1:33.3 case from the Raman spectrum. This result implies the nitridation treatments can promote the defect density in the catalysts caused by the anchored implementation of single-atom Co and N dopants in the carbon structure, which is widely believed to favor increasing the number of active sites for many catalytic reaction such as electrocatalytic water splitting. (Ref: Fei, H. *et al.* Atomic cobalt on nitrogen-doped graphene for hydrogen generation. *Nat Commun.* **6** 8668, doi:10.1038/ncomms9668, (2015).)

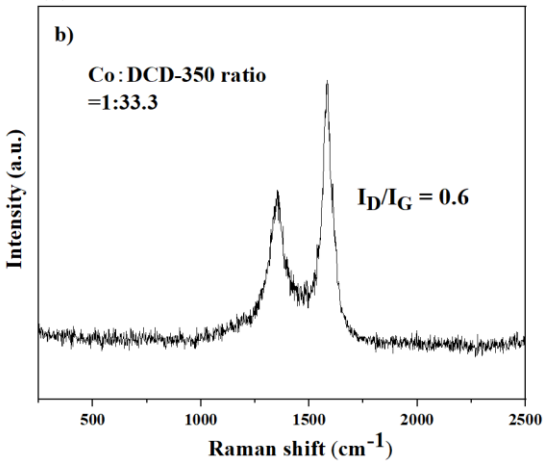

The following texts have been added to the manuscript:

In line 481,

This could explain the defect of the nanotube was due to nitridation.

3. For the amount of cobalt added, the ratio to DCD-350 was increased from 1:200 to 1:33.3. How do you determine this ratio?

Reply: Thanks. According to the Protocol 2.1, the weight ratio of $Co(acac)_2$: melem-C_3N_4 = 1:200 was mentioned. This means that *nominal* Co wt% is 0.5 wt% for 1:200 and Co wt% is 3 wt% for 1:33.3. Of course, according to the ICP-OES, the tru wt% of Co is determined to be 25.1 wt%. It was being further clarified, as in the following texts.

In line 476:

Increasing the *nominal* ratio of Co precursor to DCD-350 from 1:200 to 1:33.3 greatly impact the final morphology of the CNT catalysts.

4. The manuscript states that the synergies between NPS and SAs on the catalyst carrier are specific to the type of reaction. So what kind of synergy is for the manuscript? What stands out for this type of response?

Reply: Synergies between NPS and SAs on the catalyst carrier are specific to reaction type, and therefore whether using NPs, SAs or both depends on different reactions and different conditions. Recently, more and more attention has been paid to the research of the synergistic effect of single atom sites and nanoparticles. Apart from the example of Pd_{1+NPs}/TiO_2 mentioned in the manuscript, recently, more and more reaction made use of the NPS and SAs synergy to demonstrate superior reactivity. Other examples include the Mo SAs and Mo_2C NPs on CNTs for the N_2 reduction to ammonia, Ru NPs supported on Ni SAs confined nanotube for the highly efficient wet air oxidation of acetic acid, integrated Co SAs and Co_9S_8 NPs on CNT for electrocatalytic water splitting. All of these examples demonstrated the fact that using both SAs and NPs is better than using either one alone. In our system, the mechanism is proposed to be Co SAs responsible for water molecule adsorption and the Co NPs responsible for AB activation. In fact, we have prepared pure Co Sac-doped CNT for the AB hydrolysis and only very slow reactivity was observed. This serves the first example of using NPS and SAs synergy in the field of AB hydrolysis research.

Reference:

Ma, Y. *et al.* Synergizing Mo Single Atoms and Mo_2 C Nanoparticles on CNTs Synchronizes Selectivity and Activity of Electrocatalytic N2 Reduction to Ammonia. *Adv Mater.* **32** (33), e2002177, doi:10.1002/adma.202002177, (2020).

Jin, C. *et al.* Single-atom nickel confined nanotube superstructure as support for catalytic wet air oxidation of acetic acid. *Communications Chemistry.* **2** (1), doi:10.1038/s42004-019-0239-8, (2019).

Li, Y. *et al.* Simultaneously Integrating Single Atomic Cobalt Sites and Co9 S8 Nanoparticles into Hollow Carbon Nanotubes as Trifunctional Electrocatalysts for Zn-Air Batteries to Drive Water Splitting. *Small.* **16** (10), e1906735, doi:10.1002/smll.201906735, (2020).

5. What effect does the addition of nitrogen atoms have on the catalyst? What does it do in the reaction?

Reply:

Nitrogen (N) doped carbon nanomaterials have widely been adopted for highly enhanced (oxygen reduction reaction) ORR activity (Ref: Wei, J. *et al.* Nitrogen-Doped Nanoporous Carbon/Graphene Nano-Sandwiches: Synthesis and Application for Efficient Oxygen Reduction. *Advanced Functional Materials.* **25** (36), 5768-5777, doi:10.1002/adfm.201502311, (2015).), because the doped N atoms would produce enriched active sites (e.g. pyridinic N and graphitic N) for ORR, create anchoring accessible sites for metal crystal deposition/coordination, and efficiently modulate the intrinsically electronic property and surface chemistry of carbon structures to make the inert conjugated p electrons active towards ORR (Ref: Lai, Q. *et al.* Directly Anchoring Highly Dispersed Copper Sites on Nitrogen-Doped Carbon for Enhanced Oxygen Reduction Electrocatalysis. *ChemElectroChem.* **5** (14), 1822-1826, doi:10.1002/celc.201800058, (2018).). In this case, the N atom is believed to anchor the Co single atom on the carbon nanotube.

On the other hand, the electron transfer from Co_4N nanoparticles to the carbon atoms in N-CNTs then further to the nitrogen atoms, along with the electron transfer from single-atom Co to nitrogen atoms, leads to the Co_4N nanoparticles and single-atom Co being electron-deficient regions, while N-CNTs are electron-rich regions. This may be beneficial for rapid H_2O molecule adsorption by the Co single atom on the catalyst surface. (Ref: Cao, B. *et al.* Tailoring the *d*-band center of N-doped carbon nanotube arrays with Co_4N nanoparticles and single-atom Co for a superior hydrogen evolution reaction. *NPG Asia Materials.* **13** (1), doi:10.1038/s41427-020-00264-x, (2021).)

6. What happened to the morphology after the stability test?

Reply: Thanks for the comments. We have repeated the reaction and analyze the XRD pattern of the catalysts after 15 times of reaction run. It showed that there is no observable changes compared with the original samples before run.

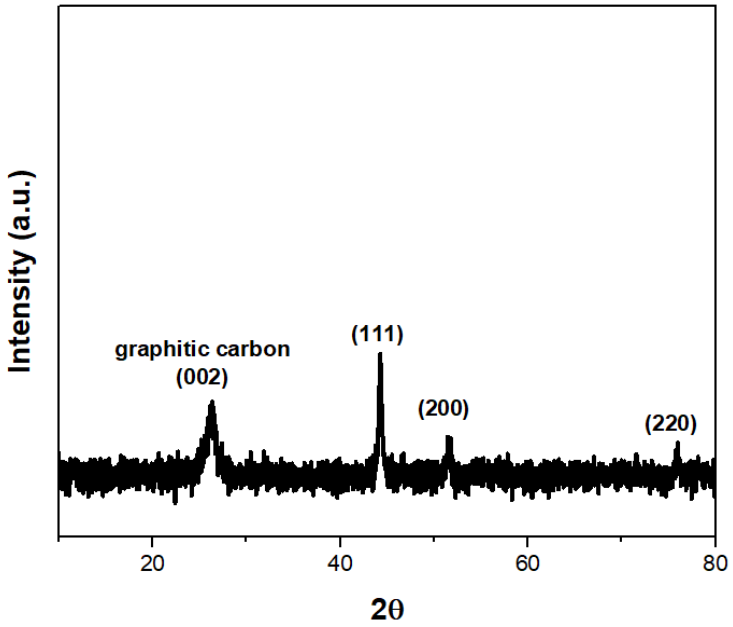

7. How to measure the amount of H_2 produced? The hydrogen generation efficiency should be offered.

Reply:

The measurement of H_2 release from AB hydrolysis was detailed in Protocol 3 and the usual water-filled inverted cylinder system was used, as show below:

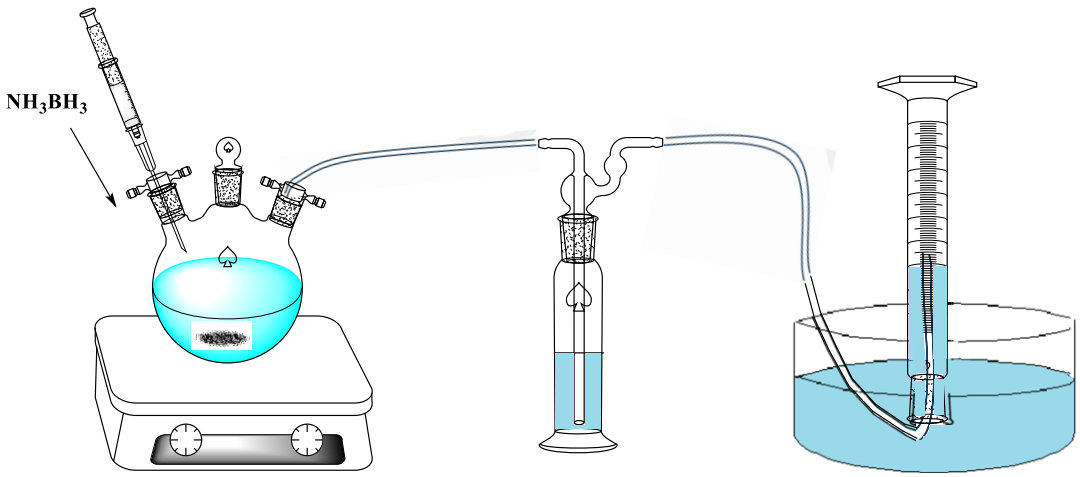

The details will be shot in the video as well.

Generally, in the research community of ammonia borane hydrolysis, the term "specific rate of hydrogen generation rate" was commonly used. We believe, in a certain extent, this is equivalent to "hydrogen generation efficiency".

8. What is the function of Co in the hydrolysis of aminoborane in the composite structure?

Reply: Numerous studies have shown that the nanoparticles are the site for AB activation through the coordination of the B-H bond to the metal centres. While after activated under alkaline media, the Co SAs will adsorb a molecule of H_2O through the oxygen atom and another Co SAs capture the proton from the H_2O. The B-H* and the Co-H* will then combine to desorb the 1st molecule of hydrogen. Consequently, the following H_2O molecules will be further activated and interact with the activated H of the B−H bond in AB, producing 3 equiv of H_2 in total.

Please see, for example:

Li, Z. *et al.* Atomically Dispersed Pt on the Surface of Ni Particles: Synthesis and Catalytic Function in Hydrogen Generation from Aqueous Ammonia–Borane. *ACS Catalysis.* **7** (10), 6762-6769, doi:10.1021/acscatal.7b01790, (2017).

Wang, Q. *et al.* Dramatic Synergy in CoPt Nanocatalysts Stabilized by "Click" Dendrimers for Evolution of Hydrogen from Hydrolysis of Ammonia Borane. *ACS Catalysis.* **9** (2), 1110-1119, doi:10.1021/acscatal.8b04498, (2018).

Cao, L. *et al.* Identification of single-atom active sites in carbon-based cobalt catalysts during electrocatalytic hydrogen evolution. *Nature Catalysis.* **2** (2), 134-141, doi:10.1038/s41929-018-0203-5, (2018).

9. The authors should be added to the latest catalyst to protrude the superiority of the nanostructures Co catalyst in the hydrolysis of aminoborane.

Reply: Thanks for the suggestion. The following texts have been added to the introduction part of the manuscript:

Recently, catalysts with hollow micro/nanostructures have been exploited for AB hydrolysis. These materials are conventionally prepared by hydrothermal methods and have been widely used for lithium-ion batteries, supercapacitors, chemical sensor and heterogeneous catalysis research. Thus, the copper-cobalt synergy towards AB hydrolysis has been demonstrated by the hollow $CuMoO_4$-$CoMoO_4$ [25], which give a high TOF of 104.7 min^{-1}. Other highly structural-dependent examples such as the core-shell CuO-NiO/Co_3O_4 [26], the $Co_xCu_{1-x}Co_2O_4$@$Co_yCu_{1-y}Co_2O_4$ yolk-shell type [27] and the $Ni_{0.4}Cu_{0.6}Co_2O_4$ nanoarrays [28] were also found to be active towards AB hydrolysis. Another type of emerging materials known as the heterostructured catalysts such as MXenes and layered double hydroxides (LDHs) are increasingly being exploited for electrocatalytic and photocatalytic reaction [29-32]. These materials such as the NiFe-layered double hydroxide [33,34] and the CoB-N materials having N-doped carbon-cobalt boride heterointerfaces [35] are especially active for oxygen evolution and reduction reaction. In principles, they could be further exploited for hydrogen evolution reaction from hydrogen storage materials such as ammonia borane [36]. Maximizing the interaction between the catalysts and substrates is also another strategy for AB hydrolysis. Chiang et al. have utilized the surface oxide group of graphene oxide to form an initiated complex species with AB [37], thus $Ni_{0.8}Pt_{0.2}$/GO and rGO demonstrated excellent reactivity towards AB hydrolysis. The use of α-MoC as support for Co and Ni single atom catalysts assisted the activation of water molecules and achieved high TOF towards AB hydrolysis, which is four times higher than the commercial Pt/C catalyst [38].

Supplementary Figure 1

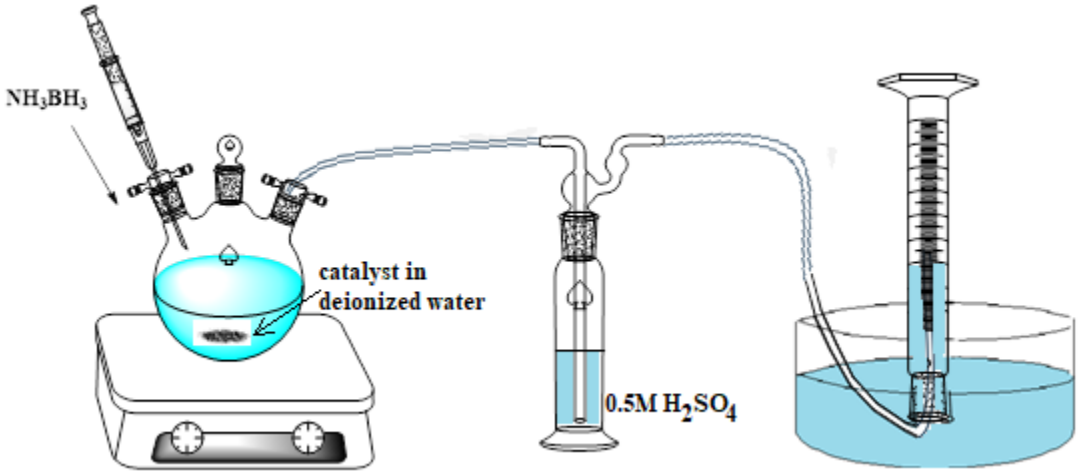

Supplementary Figure 2